Bachelor Thesis

Driven oscillations in a Fabry-Pérot cavity

Author:
David Kok

Supervisors:
Hedwig Eerkens
Dr. Martin van Exter
Dr. Vivi Rottschäfer

August 23, 2013

Universiteit Leiden

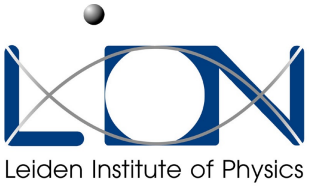

Abstract

A Fabry-Pérot cavity is a set of two mirrors which can trap light in between them. By allowing one of the two mirrors to move we find that light inside the cavity affects the mirror (through photon pressure) and the mirror affects the light (through interference between different segments of the trapped light). This coupling can be used to inhibit the motion of the mirror. This process is called laser cooling. In this thesis we investigate the behaviour of this opto-mechanically coupled system to better understand the cooling for large mirrors.

Acknowledgements

I wish to express my very great appreciation to my direct supervisor Hedwig Eerkens for her guidance and help throughout my research project. In addition I would like to thank Vivi Rottschäfer and Martin van Exter for their continuous support and constructive suggestions for the project.
My special thanks are extended to Sven de Man and Frank Buters for the insights I got from their advice.
Finally I would like to thank the other members of the Quantum Optics group for their support with my experiments and all the fruitful discussions we had.

Contents

1 Introduction

A Fabry-Pérot cavity consists of two mirrors facing each other, allowing light to be trapped between them. This configuration of mirrors was introduced by Charles Fabry and Alfred Pérot in 1897 (an introduction on Fabry-Pérot cavities and their properties can be found in several textbooks, such as [1, p. 744-776] and [2, p. 109-122]). The amount of light that can be trapped between the two mirrors depends greatly on the wavelength (and therefore on the frequency) of the light. This sensitivity is due to interference between different components of the light undergoing multiple reflections. If the wavelength of the light does not neatly fit into the cavity the light will, after a round trip through the cavity, destructively interfere with the component of the light that just entered the cavity.

This sensitivity has many applications. Fabry-Pérot cavities have found uses in for example the fabrication of lasers [3], accurate determination of the wavelength of emitted light [4] as well as filtering incoming light in astronomy [5], and gravitational wave detection [6].

In this thesis we will explore the consequences of allowing one of the mirrors of a Fabry-Pérot cavity to move on the end of a spring. We will only consider the classical regime. The light inside the cavity will provide a photon pressure (this is explained in more detail in subsection 3.3), pushing the mirror outward. But this will change the length of the cavity, thus greatly influencing the amount of light that can be stored inside the cavity. This back-and-forth interaction between the light and the movable mirror is called an opto-mechanical coupling.

In previous literature [7, 8] it has been shown that under certain circumstances this coupling can be used to restrict the movement of the mirror, lowering its effective temperature. This optical cooling or laser cooling presents a possible method of cooling macroscopic objects to their quantum mechanical ground state. Overviews of optical cooling and the field of cavity opto-mechanics can be found in [9, 10]. This thesis presents preparatory work for achieving this cooling in a large cavity with a slow mirror. In the future our goal is to apply this technique to cool a movable mirror to the quantum ground state. This cavity will be placed in one arm of a Michelson interferometer, where the other arm has a similar cavity with a fixed mirror. Upon sending a single photon into this interferometer we expect the photon to enter a state of superposition between the two arms of the interferometer. In the arm with the opto-mechanical cavity the photon will entangle with the movable mirror, thus placing a macroscopic object (the mirror) in a superposition [11].

Outline

In section 2 we will introduce the notation used throughout the thesis and present the main equations determining the evolution of the system. Furthermore we present the critical assumptions that were made in deriving these equations. Lastly we present a short summary of the conclusions from sections 3, 4 and 5.

In section 3 we present derivations of the governing equations presented in section 2. Sections 4 and 5 explore the systems of equations that we have used to describe the experiment and present theoretical conclusions on stability of critical points.

Next, section 6 presents three computer simulations. The first simulation compares the two systems of equations we have found to describe our setup. The second simulation imitates the conditions of our actual measurement, and will be used in section 9 to compare the measurement and the theory. The third simulation illustrates interesting behaviour predicted in subsection 5.2.

In section 7 we present the specifications and details of the experiment, and section 8 presents a part of the data acquired with this setup. In section 9 we compare this data with the theory as well as interpret the data.

Section 10 reinterprets our results in the light of other work on Fabry-Pérot cavities with an opto-mechanical coupling. Lastly we present a concise summary of our conclusions and some suggestions for future research in section 11.

Suggested order of reading and dependence on prerequisite knowledge

In this subsection we report on the connections between the chapters and describe what level of familiarity the reader is assumed to have with relevant theory. This is especially helpful for readers who do not have a background in both mathematics and physics.

Sections 2 and 3 require no prior knowledge of the subject matter other than basic knowledge of Taylor approximations and the notation used in differential equations. Sections 4 and 5 extend on section 3 and assume the reader to be familiar with linearised systems of differential equations around critical points. Section 6 makes use of results from sections 3, 4 and 5 but can be read after reading only section 2.

Sections 7 requires no prior knowledge. Section 8 assumes knowledge of TEM_{mn} modes of propagating light, but most of the relevant information on this is presented in appendix B. Also knowledge of Fourier transforms is required for this section. Section 9 interprets results from sections 6, 7 and 8, but can be read without reading section 6. Section 10

makes use of results of sections 4 and 5 but can be read without any prior knowledge. Lastly section 11 makes use of results from all other sections, but can be read without having read the other sections first.

It is of course recommended to read all sections, in the order they are presented. However, readers with special interest in the experimental results can safely skip sections 3 through 6, and readers with special interest in theoretical investigation can disregard sections 7 through 9.

2 Theory

2.1 Introduction

In this subsection we will introduce all variables and the most important equations used to model the experimental configuration. Also we will list the important assumptions made in deriving these equations. The detailed derivations of these equations can be found in section 3. At the end of the subsection the reader can find a list explaining all variables used in this thesis.

We are interested in a Fabry-Pérot cavity where the back mirror can move on a spring. A schematic overview is presented in figure 1:

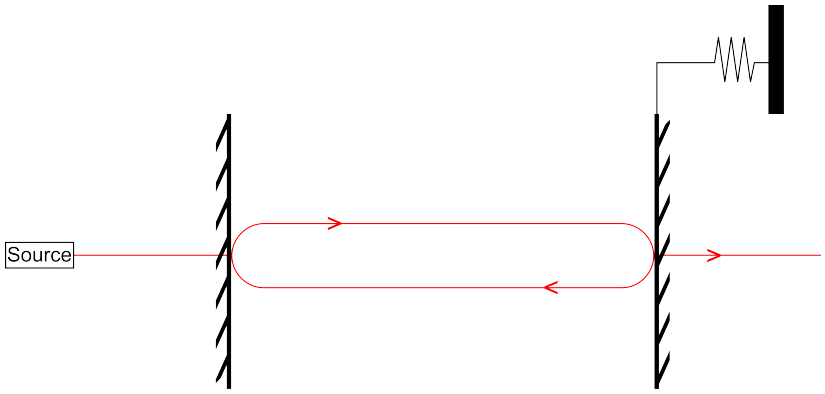

Figure 1: Schematic overview of a Fabry-Pérot cavity with a movable mirror.

We can model the moving spring as a damped harmonic oscillator with a photon pressure external force. We introduce the mirror displacement from the rest position $x(t)$, and the amplitude of the light at the surface of the moving mirror $\mathcal{A}(t)$. Also we introduce $A(t)$, which is $\mathcal{A}(t)$ in a frame rotating along with the source (i.e $A(t) = \mathcal{A}(t)e^{i\omega t}$ where ω is the frequency of the source). The reason for introducing this is that the system involves a source with an input of $Be^{-i\omega t}$ into the system, and we expect the amplitude of the light in the cavity to rotate along with this source. Therefore it is only meaningful to search for critical points, which we will do later, after we have eliminated this rotation. In subsection 3.3 we show that with this model the law of motion governing the oscillator is given by:

$$\ddot{x} + \Gamma_m \dot{x} + \Omega_m^2 x = \frac{2r_2^2}{m_{\text{eff}}c}|A(t)|^2. \tag{1}$$

Here m_{eff} is the effective mass of the mirror, $\Gamma_m m_{\text{eff}}$ is the frictional constant of the mirror system, Ω_m is the resonance frequency (so $m_{\text{eff}}\Omega_m^2$ is the spring constant of the system), r_2 is the amplitude reflection coefficient of the moving mirror and c is the speed of light.
Classically we can represent the light as photons bouncing back and forth between the

mirrors. We introduce the round trip time $\tau(t)$, which is the time it takes a photon to bounce back and forth between the two mirrors precisely once, ending at the moving mirror at time t. The round trip time is a function of time since one of the mirrors is moving (this is explained in more detail in subsection 3.1). We next note that the amplitude of the light at time t can be written as a sum of the amplitude of the light at time $t - \tau(t)$, which has just finished a round trip through the cavity, and the light added from the source. We find the following equality (the derivation of this is presented in subsection 3.1):

$$A(t) = A(t - \tau(t)) \exp\left(\left[-\frac{\kappa(t)}{2} + i\omega\right]\tau(t)\right) + Bt_1 \exp\left(\left[-\alpha + i\frac{\omega}{c}\right](L + x(t))\right). \quad (2)$$

Here $\kappa(t)$ and α are optical loss parameters, B is the amplitude of the light source (evaluated just before the surface of the fixed mirror) and t_1 is the amplitude transmission coefficient of the fixed mirror.

Another method of describing the evolution of the light inside the cavity can be found by using an approach more closely resembling Quantum Mechanical methods, and computing the commutator of A with the classical Hamiltonian to determine the time derivative of A. This leads to a differential equation, and in subsection 3.2 we present steps for deriving this differential equation from the difference equation given above. The differential equation resulting from this approach is:

$$\dot{A} = A\left[-\frac{\kappa}{2} + i\delta\omega(t)\right] + B\frac{t_1 \exp\left(\left[-\alpha + i\frac{\omega}{c}\right]L\right)}{\tau}. \quad (3)$$

Here $\delta\omega(t)$ is the time-dependent mismatch between the (time-dependent) fixed cavity resonance frequency $\omega_n(t) \approx \frac{\pi nc}{L+x(t)}$ and the source frequency ω, so $\delta\omega(t) = \omega - \omega_n(t)$.
Important to note is that these two equations do not give the same solution $A(t)$. This is not easily seen, and is shown in detail in appendix A. This incompatibility of approaches is caused by approximations made in deriving the equations; modelling the light as bouncing particles for the difference equation approach and fixing a cavity mode (i.e. setting $\omega \approx \omega_n(t)$ for some fixed n) for the differential equation. It is at this point not clear which system of equations will produce more accurate results, and in this thesis we will investigate both.

We expect the formulas presented above to be good approximations of the actual behaviour only when certain conditions are met. The effects neglected and important assumptions made to derive the equations are:

- The displacement of the mirror needs to be small, to approximate the mirror system with a damped harmonic oscillator.
- No Doppler effects from the moving have been taken into account, but might be implicit in our derivation of the equations.
- To derive the differential equation we assume that $|x(t)| \ll L$ to linearise the time-dependent resonance frequency $\omega_n(t)$ around a fixed frequency.
- To derive the differential equation we assume that the number of wavelengths the mirror moves over per round trip time is negligible, i.e. $\left|\frac{x(t)-x(t-\tau(t))}{\lambda_n(t)}\right| \ll 1$, where $\lambda_n(t) = \frac{c}{\omega_n(t)}$ can be approximated by the wavelength of the source as $\omega_n(t) \approx \omega$.
- We also assume that $|x(t)| \ll \frac{c}{\omega}$ to approximate the source contribution in the differential system with a constant. This assumption is almost equivalent to the one directly above.

To summarize, our system can be described with the following parameters:

L	Length of the system at rest (average distance between mirrors).
$x(t)$	Displacement of mirror on the spring from average position.
c	Speed of light.
m_{eff}	Effective mass of the mirror.
Γ_m	Frictional constant of the oscillating system, divided by m_{eff}
Ω_m	Resonance frequency of the mechanical system
ω	Frequency of the source (laser).
B	(Complex) Amplitude of the light wave of the source (assumed to be constant).
$\mathcal{A}(t)$	(Complex) Amplitude of the light inside the cavity, normalized so that $\lvert\mathcal{A}(t)\rvert^2$ is power.
$A(t)$	$\mathcal{A}(t)$ in a particular rotating frame, equal to $\mathcal{A}(t)e^{i\omega t}$.
r_i	(Amplitude) Reflection coefficient of mirror i (here $i = 1, 2$).
t_i	(Amplitude) Transmission coefficient of mirror i ($i = 1, 2$).
α	Loss rate (in m^{-1}) of the medium in the cavity.
$\omega_n(t)$	(Linearisation of) Time-dependent n'th resonance frequency of the cavity.
	Equal to $\frac{\pi nc}{L} - \frac{\pi nc}{L^2}x(t)$.
$\delta\omega(t)$	Mismatch between the source frequency and a fixed resonance frequency.
	Equal to $\omega - \omega_n(t)$ for some fixed n.
Δ	Detuning of the system - a first-order approximation of the mismatch.
	Equal to $\omega - \frac{\pi nc}{L}$.
$\tau(t)$	Time-dependent round trip time of the light.
	Equal to $\frac{1}{c}\left[2L + x(t) + x(t - \tau(t))\right]$, as discussed in subsection 3.1.
$\kappa(t)$	(Twice the) Averaged loss rate (in s^{-1}) of the medium in the cavity.
	Equal to $2\left(\alpha c - \frac{1}{\tau(t)}\log(r_1 r_2)\right)$.

2.2 Results

This subsection contains a summary of the main results from the mathematical chapters (sections 3, 4 and 5) and the numerical results (chapter 6).

In section 4 we show that the number of critical points in the system with the difference equation depends greatly on the relative sizes of α and ω, and that in limiting cases the difference system can have arbitrarily many critical points. We are unable to draw any conclusions about the stability of these points.

In section 5 we show that the differential system has two regimes with one critical point, and in between them a regime with three critical points. We show of one of the critical points in the regime with three critical points that it is unstable. Using numerics we show that for low power ($|B|^2$) the unique critical point of the system is stable, and that in the regime with three critical points the other two are stable, so this regime is bistable. Lastly we show the existence of Hopf bifurcations in the differential system.

Using a computer simulation we show in subsection 6.1 that the two different systems for describing the system, as mentioned above, are in good agreement. However, in appendix A we explain that there are some important differences between the two systems when x becomes large. This can occur if $|B|$ is large, causing a large photon pressure on the mirror. The simulation in subsection 6.3 mentions that the bistable regime, the regime where the differential system and the system with the difference equation might not be in agreement, is found around a value of $|B|^2 = 2.29 \cdot 10^7$ W, where we have picked realistic values for all other parameters. We conclude that in practice both systems will adequately describe the setup.
In some literature [9, 10, 12] it is claimed that if $\Delta > 0$ the solution of the system will not converge to a fixed point, so the mirror will remain in motion. In subsection 5.2 we show the existence of stable critical points in this regime, but we are unable to draw conclusions about the global convergence of solutions. This is discussed in more detail in chapter 10.

3 Derivation of governing equations

3.1 Difference equation

We consider the development of the amplitude of the light over a single round trip through the cavity. Suppose a group of photons, in our model represented by a non-zero amplitude of light $\mathcal{A}$, are present in the cavity. We assume that they start at the surface of the moving mirror, just before reflection, at time t_0. First these photons will partially reflect on the mirror (some will be transmitted and some might be absorbed), so the resulting amplitude of photons travelling back in the cavity equals the original amplitude multiplied by r_2. Next the photons will travel towards the fixed mirror at the speed of light, so they will arrive there at $t_0 + \frac{L+x(t_0)}{c}$. During this movement the amplitude of the light decreases by $\exp(-\alpha(L + x(t_0)))$ due to diffraction. At the fixed mirror the group of photons again partially get reflected, so the amplitude gets multiplied by r_1.

At this point we need to introduce the time t_1 as a function of $t_0 + \frac{L+x(t_0)}{c}$. This t_1 is the time it takes to get to the moving mirror from the fixed mirror. This time is determined by setting $ct_1 = L + x\left(t_0 + \frac{L+x(t_0)}{c} + t_1\right)$, or $t_1 = \frac{L+x\left(t_0+\frac{L+x(t_0)}{c}+t_1\right)}{c}$. The amplitude decreases with a factor similar to what was presented above, and the photons will (partially) be reflected at the moving mirror. Just before reflection the contribution from the source is added, which we will discuss below.
We introduce the end time $t_{\text{end}} = t_0 + t_1 + \frac{L+x(t_0)}{c}$. Using this we can write the (complex) amplitude of the blob after a round trip, temporarily ignoring the contribution from the source, as:

$$\mathcal{A}_{\text{end}} = \mathcal{A} r_1 r_2 \exp\left(-\alpha(2L + x(t_0) + x(t_{\text{end}}))\right).$$

We can write this in a more readable form by introducing the round trip time $\tau(t)$. It is practical to define the round trip time backwards, i.e. $\tau(t)$ is such that a round trip that started at the surface of the moving mirror at time $t - \tau(t)$ finishes precisely at time t. Using this we can write:

$$c\tau(t) = 2L + x(t) + x(t - \tau(t)).$$

Note that, in our notation above, we have $t_{\text{end}} = t_0 + \tau(t_{\text{end}})$. Using this we can rewrite the expression above for A_{end} as:

$$\mathcal{A}(t) = \mathcal{A}(t - \tau(t)) r_1 r_2 \exp(-\alpha c \tau(t)).$$

Lastly we introduce the averaged loss rate $\kappa(t)$ through:

$$\kappa(t) = 2\left(\alpha c - \frac{1}{\tau(t)} \log(r_1 r_2)\right).$$

Here the factor 2 is for conventional purposes, it is common to let κ denote the loss rate of power, which is twice the loss rate of amplitude. Using this we can rewrite the equation

above to:

$$\mathcal{A}(t) = \mathcal{A}(t - \tau(t)) \exp\left(-\frac{\kappa(t)}{2}\tau(t)\right).$$

We now consider the source contribution. We demand that the contribution from the source arrives at the moving mirror at time t. We assume the source to have a known complex amplitude of $Be^{-i\omega t}$ at time t, located just before the surface of the fixed mirror. Since the source contribution arrives at the moving mirror at time t, and it travels at the speed of light, it was transmitted through the fixed mirror at time $t - \frac{L+x(t)}{c}$. The phase of the source contribution is therefore equal to $-\omega\left(t - \frac{L+x(t)}{c}\right)$. Lastly the amplitude of the source term suffers losses equal to $t_1 \exp\left(-\alpha(L + x(t))\right)$ before arriving at the surface of the moving mirror, again due to diffraction. Combining this with the equation above yields:

$$\mathcal{A}(t) = \mathcal{A}(t-\tau(t)) \exp\left(-\frac{\kappa(t)}{2}\tau(t)\right) + Bt_1 \exp\left(-\alpha(L + x(t))\right) \exp\left(-i\omega\left(t - \frac{L + x(t)}{c}\right)\right).$$

At this point we introduce the amplitude of the light in a particular rotating frame, as discussed in subsection 2.1; $A(t) = \mathcal{A}(t)e^{i\omega t}$. From substituting this in the equation above we get:

$$A(t)e^{-i\omega t} = A(t - \tau(t))e^{-\frac{\kappa(t)}{2}\tau(t)}e^{-i\omega(t-\tau(t))} + Bt_1 e^{-\alpha(L+x(t))}e^{-i\omega\left(t-\frac{L+x(t)}{c}\right)}.$$

We next multiply this equation by $e^{i\omega t}$ to obtain:

$$A(t) = A(t - \tau(t)) \exp\left(\left[-\frac{\kappa(t)}{2} + i\omega\right]\tau(t)\right) + Bt_1 \exp\left(\left[-\alpha + i\frac{\omega}{c}\right](L + x(t))\right). \quad (2)$$

3.2 Differential equation

In this section we will present some steps for converting equation 2 to a first-order differential equation. Important to note is that the difference equation presented above is far more complex than a first-order differential equation. This can for example be seen by looking at the initial conditions required to uniquely determine a solution: a first-order differential equation requires only a single initial condition, whereas the difference equation 2 above requires a whole interval $-\tau(0) < t < 0$ as initial conditions. We therefore do not expect to be able to properly derive a differential equation from equation 2.

However, we are trying to model a physical system involving light, which under many commonly found circumstances is better described by waves than by particles. Modelling the light in the cavity as waves would lead us to describe the evolution of the light in the cavity with a differential equation, presumably first-order and linear. It is therefore worth

searching for a differential equation that is (approximately) compatible with equation 2, and in this section we will try to derive a differential equation from equation 2.

In order to do this we first need to introduce a few more variables. We introduce the first-order approximation of the instantaneous resonance frequencies:

$$\omega_n(t) = \frac{\pi nc}{L} - \frac{\pi nc}{L^2}x(t) \approx \frac{\pi nc}{L + x(t)}$$

Note that it would be a bit more neat to introduce $\omega_n(t)$ as the actual instantaneous resonance frequencies, but the approximation above is more convenient for calculations and will give rise to similar dynamics as long as $|x| \ll L$. We expect this assumption to be justified as the photon pressure in typical experiments is low, so $|x|$ will be small.

We will from here on assume that the frequency of the source, ω, is chosen near a certain resonance frequency $\frac{\pi nc}{L}$, and fix that n. Using this we can introduce the instantaneous mismatch $\delta\omega(t) = \omega - \omega_n(t)$, and we also introduce the detuning $\Delta = \omega - \frac{\pi nc}{L}$. We substitute $\omega = \delta\omega(t) + \omega_n(t)$ and $\tau(t) = \frac{1}{c}\left[2L + x(t) + x(t - \tau(t))\right]$ in equation 2 to get:

$$A(t) = A(t-\tau(t))e^{-\frac{\kappa(t)}{2}\tau(t)}e^{i(\omega_n(t)+\delta\omega(t))\left(\frac{1}{c}[2L+x(t)+x(t-\tau(t))]\right)} + Bt_1 e^{i\omega\frac{1}{c}(L+x(t))}e^{-\alpha(L+x(t))}.$$

Note that $\omega_n(t)$ is defined in such a way that $e^{i\omega_n(t)\frac{1}{c}(2L+2x(t))} = 1$ (up to first order in x), so we can rewrite the above to:

$$\begin{aligned} A(t) &= A(t-\tau(t))e^{-\frac{\kappa(t)}{2}\tau(t)}e^{i\left(\frac{\omega_n(t)}{c}[x(t-\tau(t))-x(t)]+\frac{\delta\omega(t)}{c}[2L+x(t)+x(t-\tau(t))]\right)} + Bt_1 e^{i\omega\frac{1}{c}(L+x(t))}e^{-\alpha(L+x(t))} \\ &= A(t-\tau(t))e^{-\frac{\kappa(t)}{2}\tau(t)}e^{i\left(\frac{\omega_n(t)}{c}[x(t-\tau(t))-x(t)]+\delta\omega(t)\tau(t)\right)} + Bt_1 e^{i\omega\frac{1}{c}(L+x(t))}e^{-\alpha(L+x(t))}. \end{aligned}$$

At this point we ignore the $\frac{\omega_n(t)}{c}\left[x(t-\tau(t)) - x(t)\right]$-term, although it is not really clear whether or not this is allowed. We expect x to be roughly constant over times of $\tau(t)$, in which case the term would drop out, but a complete justification is lacking.
By ignoring the term we can reduce this equation to the equation below:

$$A(t) = A(t-\tau(t))\exp\left(\left[-\frac{k(t)}{2} + i\delta\omega(t)\right]\tau(t)\right) + Bt_1\exp\left(\left[-\alpha + i\frac{\omega}{c}\right](L + x(t))\right).$$

This difference equation resembles the differential equation found in literature, so we will next attempt to construct a differential equation from this difference equation. Our attempts at this have not been completely successful, but we will outline the general idea below:

Suppose we have a delay equation of the form

$$A(t) = A(t-\tau)e^{\lambda T} + b.$$

where τ, λ, b are constants, and $\lambda\tau \neq 0$. We will first shift this A to remove the constant b from this equation. We do this by introducing $d = \frac{b}{e^{\lambda\tau}-1}$ and $C(t) = A(t) + d$. Note that

$$d + b = \frac{b}{e^{\lambda\tau}-1} + b = \frac{b\left(1 + e^{\lambda\tau} - 1\right)}{e^{\lambda\tau}-1} = e^{\lambda\tau}d.$$

From this it follows that:

$$\begin{aligned} C(t) &= A(t) + d \\ &= A(t-\tau)e^{\lambda\tau} + b + d \\ &= A(t-\tau)e^{\lambda\tau} + e^{\lambda\tau}d \\ &= e^{\lambda\tau}C(t-\tau). \end{aligned}$$

We therefore expect[1] that $C(t) = C(0)e^{\lambda t}$, and that $\frac{dC}{dt} = \lambda C$. We can find this equation in a few steps, first by taking the logarithm of both sides to get:

$$\log(C(t)) = \log(C(t-\tau)) + \lambda\tau.$$

Next we construct a Taylor expansion of $\log(C(t-\tau))$ around $\tau = 0$:

$$\log(C(t)) = \log(C(t)) - \tau\frac{\frac{dC}{dt}}{C} + O(\tau^2) + \lambda\tau.$$

In order for this Taylor expansion to be a good approximation of the actual logarithm we need that τ is small when compared to $\frac{C}{\frac{dC}{dt}}$, i.e. that C (and therefore A) does not change much over timescales on the order of τ. In the actual experiment this would mean that the light in the cavity does not fluctuate heavily over a single round trip, which we expect to be the case.

In the equation above the $\log(C(t))$ cancels and, ignoring all $O(\tau^2)$ or higher terms, we can rewrite the equation above as:

$$\frac{dC}{dt} \approx \lambda C.$$

We next undo the substitution $C(t) = A(t) + d$ and expand the expression for d to get:

$$\frac{dA}{dt} \approx \lambda A + \frac{\lambda}{e^{\lambda\tau} - 1}b.$$

Under the assumption that $\lambda\tau \ll 1$ we can approximate the exponential with a first-order Taylor polynomial to get:

$$\frac{dA}{dt} \approx \lambda A + \frac{b}{\tau}.$$

[1] As mentioned before a difference equation is more complex than a differential equation, and it is in this step that we lose information. It does not follow from $C(t) = C(t-\tau)e^{\lambda\tau}$ that $C(t) = C(0)e^{\lambda t}$ - a simple counterexample is $C(t) = C(0)e^{\left(\lambda + \frac{2\pi i}{\tau}\right)t}$ which also satisfies the given difference equation. This can be understood by noting that a different choice of λ here creates different behaviour on timescales smaller than τ, which are not uniquely determined by the difference equation unless we have a whole interval as initial conditions. By picking a λ we are claiming that this particular λ will correctly determine the behaviour of A over a whole interval $-\tau(0) < t < 0$, an assumption required to describe the problem with a differential equation.

In our case the λ, τ and b are not constants but functions, complicating the approach given above (eliminating the constant and constructing the Taylor expansion of the logarithm present problems). Nevertheless we expect that, for functions which are well approximated by a constant, we can replace the constants with our functions without major problems. The resulting differential equation is given by:

$$\frac{dA}{dt} = A\left[-\frac{\kappa(t)}{2} + i\delta\omega(t)\right] + B\frac{t_1 \exp\left(\left[-\alpha + i\frac{\omega}{c}\right](L + x(t))\right)}{\tau(t)}.$$

Note that the solution of this differential equation will **not** satisfy the difference equation found before, as we have made some approximations (see appendix A).

In fact we will make some more simplifying assumptions. The equation above describes the evolution of the light in the cavity, and we can picture the evolution of this light as a combination of decay of the field and interference with the source. Out of these two effects the dominant effect is the interference with the source, which is determined mainly by the phases of the source and the light in the cavity. In the equation above these are determined by $\delta\omega(t)$ and $\frac{\omega}{c}(L + x(t))$. The decay of the field is represented by $-\frac{\kappa(t)}{2}$ and by $\frac{t_1}{\tau}\exp(-\alpha(L + x(t)))$.
Since these latter terms are only of minor importance we can substitute approximations for them. We will approximate $\kappa(t)$ with a constant κ, given by

$$\kappa = 2\alpha c - \frac{c}{L}\log(r_1 r_2).$$

If $x(t) = 0$ for all t this would coincide with $\kappa(t)$. If $|x(t)| \ll L$, and assumption which we expect to hold, this approximation is a good one. With an argument similar to the above we will approximate $-\alpha(L + x(t))$ with $-\alpha L$.
Lastly we will approximate $\frac{\omega}{c}(L + x(t))$ with $\frac{\omega}{c}L$. Note that in the presented differential equation this term represents the phase of the source, so we expect this approximation to be acceptable if $\frac{\omega}{c}x(t) \ll 1$. In physical terms this means that we assume that the mirror moves far less than the wavelength of the source. This is an assumption which we expect to be valid.
Lastly we will approximate $\tau(t)$ with a constant $\frac{2L}{c}$, we expect this to be justified for $|x(t)| \ll L$. Substituting these approximations results in the following differential equation:

$$\dot{A} = A\left[-\frac{\kappa}{2} + i\delta\omega(t)\right] + B\frac{t_1 \exp\left(\left[-\alpha + i\frac{\omega}{c}\right]L\right)}{\tau}. \tag{3}$$

It might seem like deriving the differential equation from the difference equation is poorly justified, and that we need to make many assumptions and approximations to get any results. Important to note is that the difference equation is burdened with the assumption that light can be represented as bouncing packets, and that a more exact model would arise from computing the Hamiltonian to determine the time evolution of A. We therefore suspect that the differential equation might be a valid approximation of the physical behaviour even if some of the demands presented above are not met.

3.3 Oscillator

In this subsection we will derive the equation governing the movement of the mirror. The mirror on the spring behaves like a damped harmonic oscillator with spring constant $k = m_{\text{eff}}\Omega_m^2$, so the force at displacement $x(t)$ equals $-kx(t)$. Furthermore there is a friction coefficient of $m_{\text{eff}}\Gamma_m$, so the force of friction equals $-m_{\text{eff}}\Gamma_m \frac{dx(t)}{dt}$. Newton's second law tells us that:

$$\begin{aligned} m_{\text{eff}}\frac{d^2x(t)}{dt^2} &= F_{\text{tot}}(t) \\ &= F_{\text{spring}}(t) + F_{\text{friction}}(t) + F_{\text{external}}(t) \\ &= -m_{\text{eff}}\Omega_m^2 x(t) - m_{\text{eff}}\Gamma_m \frac{dx(t)}{dt} + F_{\text{external}}(t) \end{aligned}$$

The external force is the photon pressure on the spring, which is given by $2r_2^2|\mathcal{A}(t)|^2\frac{1}{c}$. The power (in Watt) of the photons at time t is equal to $|\mathcal{A}(t)|^2$, as per normalisation of the amplitude (we pick our normalisation such that the above is true, and all our equations are valid as long as we pick the same normalisation for B). For a photon the momentum it has is equal to its energy divided by the speed of light c (this follows from the fact that its energy equals $E = \hbar\omega$, and its momentum equals $\hbar k$, and the phase velocity of a photon is equal to $c = \frac{\omega}{k}$). Upon reflection on a mirror the momentum of the photon changes sign, and by conservation of momentum the mirror picks up a momentum of twice that of the photon. The force acting on the mirror, which is equal to the time derivative of its momentum (by Newton's Law), is therefore equal to the energy density of the light, times 2. Only the photons which are reflected contribute to the pressure, so the term is multiplied by the power reflection coefficient, which is $|r_2|^2 = r_2^2$ since r_2 is real. By substituting this and dividing by m_{eff} we get:

$$\ddot{x} + \Gamma_m\dot{x} + \Omega_m^2 x = \frac{2r_2^2}{m_{\text{eff}}c}|A(t)|^2. \tag{1}$$

4 Stability of critical points in the difference system

4.1 Critical points

In this chapter we will first determine the critical points of the system with the difference equation, and then attempt to determine the stability of these critical points by constructing an expansion of the solution around a critical point. The system we are interested in is given by:

$$A(t) = A(t-\tau(t))\exp\left(\left[-\frac{\kappa(t)}{2}+i\omega\right]\tau(t)\right) + Bt_1\exp\left(\left[-\alpha+i\frac{\omega}{c}\right](L+x(t))\right). \quad (2)$$

$$\ddot{x}+\Gamma_m\dot{x}+\Omega_m^2 x = \frac{2r_2^2}{m_{\text{eff}}c}|A(t)|^2. \quad (1)$$

Setting $A(t)=A_c, x(t)=x_c$ and introducing $Y=\frac{2r_2^2}{c\Omega_m^2 m_{\text{eff}}}$ gives us:

$$A_c = A_c\exp\left(\left[-\frac{\kappa(t)}{2}+i\omega\right]\tau(t)\right) + Bt_1\exp\left(\left[-\alpha+i\frac{\omega}{c}\right](L+x_c)\right).$$
$$x_c = Y|A_c|^2.$$

Note that τ satisfies $\tau(t)=\frac{1}{c}\left[2L+x(t)+x(t-\tau(t))\right]$, but since $x(t)=x_c$ we can rewrite this as $\tau=\frac{2}{c}\left[L+x_c\right]$, and from this it follows that κ is also a constant. We can rewrite the above to:

$$A_c\left(1-\exp\left(\left[-\frac{\kappa}{2}+i\omega\right]\tau\right)\right) = Bt_1\exp\left(\left[-\alpha+i\frac{\omega}{c}\right](L+x_c)\right).$$

Using the equation directly above for τ, and using that $\frac{\kappa}{2}=\alpha c-\frac{1}{\tau}\log(r_1r_2)$, we can rewrite the equation above as:

$$A_c\left(1-r_1r_2\exp\left(\left[-\alpha c+i\omega\right]\frac{1}{c}\left[2L+2x_c\right]\right)\right) = Bt_1\exp\left(\left[-\alpha+i\frac{\omega}{c}\right](L+x_c)\right).$$

We next divide both sides by $\exp\left(\left[-\alpha+i\frac{\omega}{c}\right](L+x_c)\right)$ and multiply both sides with their complex conjugate to get:

$$|A_c|^2\left(e^{2\alpha(L+x_c)}+r_1^2r_2^2e^{-2\alpha(L+x_c)}-2r_1r_2\cos\left(2\frac{\omega}{c}(L+x_c)\right)\right) = |B|^2|t_1|^2.$$

Assuming that $r_1r_2\neq 0$ we can rewrite this as:

$$|A_c|^2\left(2r_1r_2\cosh\left(2\alpha(L+x_c)-\log(r_1r_2)\right)-2r_1r_2\cos\left(2\frac{\omega}{c}(L+x_c)\right)\right) = |B|^2|t_1|^2.$$

Using $x_c = Y|A_c|^2$ allows us to rewrite this as:

$$x_c \left(\cosh\left(2\alpha(L + x_c) - \log(r_1 r_2)\right) - \cos\left(2\frac{\omega}{c}(L + x_c)\right)\right) = \frac{|B|^2 |t_1|^2}{2 r_1 r_2 Y}.$$

In the experiment we consider $|B|$ and ω to be a tuneable parameters, and the value x_c can be determined from the equation given directly above. Important to note is that if $\frac{\omega}{c} \gg \alpha$ the period of the cosine is small, so the hyperbolic cosine is roughly constant over a period of the cosine. If we find a solution x_c of the equation above we therefore expect to be able to find another one almost a period further.
In particular, in the extreme case $\alpha = 0$ we find that the term between brackets reduces to $\cosh(-\log(r_1 r_2)) - \cos\left(2\frac{\omega}{c}(L + x_c)\right)$. Under the assumptions $r_1 = r_2$ and $r_1^2 + t_1^2 = 1$ we find that there is a solution with maximal x_c in the neighbourhood of $x_c = \frac{|b|^2}{Y(1-r_1^2)}$, which is quite large. We expect to find a solution every period of the cosine before this maximal solution, so in this limiting case the system has many critical points.
Conversely, if $\alpha \gg \frac{\omega}{c}$ we can approximate the cosine with a constant, and since L and x_c have the same sign we note that the hyperbolic cosine is strictly increasing. Therefore the equation above will only have one solution x_c for every value of $|B|$ under these circumstances.
We conclude that the number of critical points depends greatly on the relative sizes of α and $\frac{\omega}{c}$.

Important to note is that if we find x_c we can find A_c from the equations above. Therefore every non-negative solution x_c of the equation above gives us a single critical point. In particular we see that the number of critical points depends greatly on the value of $\frac{\omega}{c}$ compared to α.

4.2 Stability

We next wish to determine the stability of the critical points found in the previous section. In order to determine the behaviour of the system around a critical point we first split A into a real and imaginary part, $A(t) = a(t) + ib(t)$ where a, b are real functions. Write $A_c = a_c + ib_c$. Also we introduce $v = \frac{dx}{dt}$. Next we determine the behaviour of the system near a critical point $(A, x, v) = (a_c + ib_c, x_c, 0)$ by setting $(A, x, v) = (a_c + ib_c, x_c, 0) + (\tilde{a}(t) + i\tilde{b}(t), \tilde{x}(t), \tilde{v}(t))$ where $\tilde{a}, \tilde{b}, \tilde{x}$ and $\tilde{v}$ are small. Substituting this in our system of equations

yields:

$$\begin{aligned}
\frac{d}{dt}\left(x_c+\tilde{x}\right) &= (0+\tilde{v}) \\
\frac{d}{dt}\left(0+\tilde{v}\right) &= Y\left|a_c+\tilde{a}+i(b_c+\tilde{b})\right|^2-\Gamma_m(0+\tilde{v})-\Omega_m^2(x_c+\tilde{x}) \\
(a_c+\tilde{a}+i(b_c+\tilde{b}))(t) &= (a_c+\tilde{a}+i(b_c+\tilde{b}))(t-\tau(t))\exp\left(\left[-\frac{\kappa(t)}{2}+i\omega\right]\tau(t)\right) \\
&\quad + Bt_1\exp\left(\left[-\alpha+i\frac{\omega}{c}\right](L+(x_c+\tilde{x}(t)))\right).
\end{aligned}$$

Also we know that:

$$\begin{aligned}
\tau(t) &= \frac{1}{c}\left[2L+(x_c+\tilde{x})(t)+(x_c+\tilde{x})(t-\tau(t))\right] \\
\kappa(t) &= 2\left(\alpha c-\frac{1}{\tau(t)}\log(r_1r_2)\right)
\end{aligned}$$

Since $(a_c+ib_c,x_c,0)$ is a critical point of the system we know that:

$$0 = Y\left|a_c+ib_c\right|^2-\Gamma_m\cdot 0-\Omega_m^2x_c,$$

and that:

$$a_c+ib_c = (a_c+ib_c)\exp\left(\left[-\frac{\kappa_c}{2}+i\omega\right]\tau_c\right)+Bt_1\exp\left(\left[-\alpha+i\frac{\omega}{c}\right](L+x_c)\right).$$

Here we have introduced $\tau_c=\frac{1}{c}[2L+2x_c]$ and $\kappa_c=2\left(\alpha c-\frac{1}{\tau_c}\log(r_1r_2)\right)$. Next we note that:

$$\tau(t)-\tau_c = \frac{\tilde{x}(t)-\tilde{x}(t-\tau(t))}{c},$$

and that:

$$\kappa(t)-\kappa_c = -\log(r_1r_2)\left(\frac{1}{\tau(t)}-\frac{1}{\tau_c}\right).$$

Using a Taylor approximation for $\tau(t)$ around τ_c (since $\tilde{x}$ is small) we can approximate this with:

$$\kappa(t)-\kappa_c = \log(r_1r_2)\frac{\tilde{x}(t)+\tilde{x}(t-\tau(t))}{c\tau_c^2}+O(\tilde{x}^2)$$

Using this we can write:

$$\begin{aligned}\exp\left(\left[-\frac{\kappa(t)}{2}+i\omega\right]\tau(t)\right) &= \exp\left(\left[-\frac{\kappa_c}{2}+i\omega\right]\tau_c+(\tau(t)-\tau_c)\left[-\frac{\kappa_c}{2}+i\omega\right]+\left[-\frac{\kappa(t)-\kappa_c}{2}\right]\tau(t)\right)\\ &= \exp\left(\left[-\frac{\kappa_c}{2}+i\omega\right]\tau_c\right)\exp\left(\frac{\tilde{x}(t)+\tilde{x}(t-\tau(t))}{c}\left[-\frac{\kappa_c}{2}+i\omega\right]\right)\\ &\quad\cdot\exp\left(\left[\log(r_1r_2)\frac{\tilde{x}(t)+\tilde{x}(t-\tau(t))}{c\tau_c^2}\right]\tau(t)\right)\exp\left(O(\tilde{x}^2)\right).\end{aligned}$$

Note that we have $\tau(t)=\tau_c+O(\tilde{x})$ so we can (up to $O(\tilde{x})$) approximate the $\tau(t)$ in the last exponent with τ_c. We substitute this in the equation above to get:

$$\begin{aligned}\exp\left(\left[-\frac{\kappa(t)}{2}+i\omega\right]\tau(t)\right) &= \exp\left(\left[-\frac{\kappa_c}{2}+i\omega\right]\tau_c\right)\\ &\quad\cdot\exp\left(\frac{\tilde{x}(t)+\tilde{x}(t-\tau(t))}{c}\left[-\frac{\kappa_c}{2}+\frac{\log(r_1r_2)}{\tau_c}+i\omega\right]\right)\exp(O(\tilde{x}^2))\end{aligned}$$

Next we will construct a first-order Taylor polynomial of the exponent with the $\tilde{x}$ and substitute this equation in our difference equation presented earlier. After constructing a first-order Taylor expansion of the other exponent with a $\tilde{x}$ around $\tilde{x}=0$, and noting that the constant terms cancel since $(a_c+ib_c,x_c,0)$ is a critical point of the system, we obtain the following system of equations:

$$\begin{aligned}\frac{d\tilde{x}}{dt} &= \tilde{v}\\ \frac{d\tilde{v}}{dt} &= Y\left(2a_c\tilde{a}+2b_c\tilde{b}\right)-\Gamma_m\tilde{v}-\Omega_m^2\tilde{x}+O(\tilde{a}^2,\tilde{b}^2)\\ \tilde{a}(t)+i\tilde{b}(t) &= (a_c+ib_c)\exp\left(\left[-\frac{\kappa_c}{2}+i\omega\right]\tau_c\right)\left(\frac{\tilde{x}(t)+\tilde{x}(t-\tau(t))}{c}\left[-\frac{\kappa_c}{2}+\frac{\log(r_1r_2)}{\tau_c}+i\omega\right]\right)\\ &\quad+(\tilde{a}(t-\tau(t))+i\tilde{b}(t-\tau(t)))\exp\left(\left[-\frac{\kappa_c}{2}+i\omega\right]\tau_c\right)\\ &\quad+Bt_1\exp\left(\left[-\alpha+i\frac{\omega}{c}\right](L+x_c)\right)\tilde{x}(t)+O(\tilde{x}^2)\end{aligned}$$

Next we ignore all terms of $O(\tilde{a}^2,\tilde{b}^2,\tilde{x}^2)$ as $\tilde{a},\tilde{b},\tilde{x}$ are small. Worthy of note is that, up to $O(\tilde{x}^2)$, we can approximate $\tilde{a}(t-\tau(t))$ and $\tilde{b}(t-\tau(t))$ with $\tilde{a}(t-\tau_c)$ and $\tilde{b}(t-\tau_c)$ respectively by constructing a Taylor expansion around $\tau(t)=\tau_c$.

The general approach to determining the stability of this system is assuming that $(\tilde{a}(t),\tilde{b}(t),\tilde{x}(t),\tilde{v}(t))=e^{\lambda t}(\tilde{a}(0),\tilde{b}(0),\tilde{x}(0),\tilde{v}(0))$ for some $\lambda\in\mathbb{C}$ and solving for λ. Below we will present the first few steps of this approach. First we substitute the first in the second equation to get a second-order differential equation:

$$\frac{d^2\tilde{x}}{dt^2}+\Gamma_m\frac{d\tilde{x}}{dt}+\Omega_m^2\tilde{x}=Y\left(2a_c\tilde{a}+2b_c\tilde{b}\right)$$

If we now substitute the form given above and divide by $e^{\lambda t}$ we find:

$$\tilde{x}(0)\left(\lambda^2 + \Gamma_m \lambda + \Omega_m^2\right) = Y\left(2a_c\tilde{a}(0) + 2b_c\tilde{b}(0)\right)$$

Next, if we substitute the exponentials in the difference equation and divide by $e^{\lambda t}$ we get:

$$\begin{aligned}\tilde{a}(0) + i\tilde{b}(0) = (a_c + ib_c)\exp\left(\left[-\frac{\kappa_c}{2} + i\omega\right]\tau_c\right)\left[-\frac{\kappa_c}{2} + \frac{\log(r_1 r_2)}{\tau_c} + i\omega\right]\frac{1 + e^{-\lambda\tau_c}}{c}\tilde{x}(0) \\ + (\tilde{a}(0) + i\tilde{b}(0))\exp\left(\left[-\frac{\kappa_c}{2} + i\omega\right]\tau_c\right)e^{-\lambda\tau_c} \\ + Bt_1\exp\left(\left[-\alpha + i\frac{\omega}{c}\right](L + x_c)\right)\tilde{x}(0) + O(\tilde{x}^2)\end{aligned}$$

The stability of the critical points of the system is now determined by the real parts of the λ that solve the system of equations given above. Note that we have 3 real equations (since the result from the difference equation can be split into real and imaginary part) and 3 initial values $\tilde{a}(0), \tilde{b}(0), \tilde{x}(0)$ since by assumption we have $\tilde{x}(t) = e^{\lambda t}\tilde{x}(0)$ so $\tilde{v}(0) = \frac{d\tilde{x}}{dt}(0) = \lambda\tilde{x}(0)$. We therefore expect that the equations above will yield the eigenvalues we are looking for, although we were not able to actually solve for the eigenvalues.

5 Stability of critical points in the differential system

5.1 Critical points

In this chapter we will determine the limiting behaviour of the solution to the system of differential equations by finding all critical points of this system and determining their stability. The system is given below:

$$\ddot{x} + \Gamma_m \dot{x} + \Omega_m^2 x = \frac{2r_2^2}{m_{\text{eff}} c} |A(t)|^2. \tag{1}$$

$$\dot{A} = A\left[-\frac{\kappa}{2} + i\delta\omega(t)\right] + B\frac{t_1 \exp\left(\left[-\alpha + i\frac{\omega}{c}\right] L\right)}{\tau}. \tag{3}$$

Here $\delta\omega(t) = \Delta - \omega_n \frac{x(t)}{L}$ and $\omega_n = \frac{\pi n c}{L}$. Introducing the constants $Y = \frac{2r_2^2}{m_{\text{eff}} c}$ and $Z = \left|\frac{t_1 \exp\left(\left[-\alpha + i\frac{\omega}{c}\right] L\right)}{\tau}\right|$, and absorbing the phase of the constantnext to B into B, we can rewrite this system as:

$$\ddot{x} + \Gamma_m \dot{x} + \Omega_m^2 x = Y|A(t)|^2.$$
$$\dot{A} = A\left[-\frac{\kappa}{2} + i\delta\omega(t)\right] + BZ.$$

We introduce $v = \dot{x}$ and real $s(t), \theta(t), q, \phi$ (we also demand that $s(t), q \geq 0$) through $A(t) = s(t)e^{i\theta(t)}$ and $B = qe^{i\phi}$. We search for critical points of the system, where $0 = \dot{x} = \dot{v} = \dot{A}$. If we substitute these expressions it now follows that:

$$0 = \dot{x} = v$$
$$0 = \dot{v} = -\Gamma_m v - \Omega_m^2 x + Y s^2$$
$$0 = \dot{A} = s e^{i\theta}\left[-\frac{\kappa}{2} + i\left(\Delta - \omega_n \frac{x}{L}\right)\right] + Z q e^{i\phi}$$

From this it follows that:

$$x = \frac{Y s^2}{\Omega_m^2}.$$

Inserting this in the last equation yields:

$$Z q e^{i\phi} = -s e^{i\theta}\left[-\frac{\kappa}{2} + i\left(\Delta - \omega_n \frac{Y s^2}{L\Omega_m^2}\right)\right].$$

By setting the modulus of both sides equal we obtain:

$$Zq = s\sqrt{\left(-\frac{\kappa}{2}\right)^2 + \left(\Delta - \omega_n \frac{Y s^2}{L\Omega_m^2}\right)^2}.$$

By taking the square of both sides it now follows that s satisfies:

$$0 = \left(\frac{\omega_n Y}{L\Omega_m^2}\right)^2 s^6 - 2\Delta\left(\frac{\omega_n Y}{L\Omega_m^2}\right) s^4 + \left(\frac{\kappa^2}{4} + \Delta^2\right) s^2 - (qZ)^2.$$

From the earlier equation we see that it also holds that (actually we only know this equation to be true up to a multiple of 2π, but since adding a multiple of 2π to a solution θ does not change the value of A we might as well pick this particular solution):

$$\phi = \theta + \pi + \arctan\left(\frac{\Delta - \left(\frac{\omega_n Y}{L\Omega_m^2}\right) s^2}{-\frac{\kappa}{2}}\right).$$

After introducing $d_1 = \left(\frac{\omega_n Y}{L\Omega_m^2}\right) = \left(\frac{2\omega_n r_2^2}{cL\Omega_m^2 m_{\text{eff}}}\right)$ we can rewrite the equations above to:

$$0 = d_1^2 s^6 - 2\Delta d_1 s^4 + \left(\frac{\kappa^2}{4} + \Delta^2\right) s^2 - (qZ)^2.$$
$$\phi = \theta + \pi + \arctan\left(\frac{\Delta - d_1 s^2}{-\frac{\kappa}{2}}\right).$$

Here we introduce $p = s^2$, so this equation becomes a cubic polynomial in p. Note that at $p = 0$ the polynomial is negative, so by the intermediate value theorem (between $p = 0$ and $p \to \infty$) this polynomial has at least one positive root (and therefore at least one real solution for s). We present a plot of this polynomial for different values of Δ:

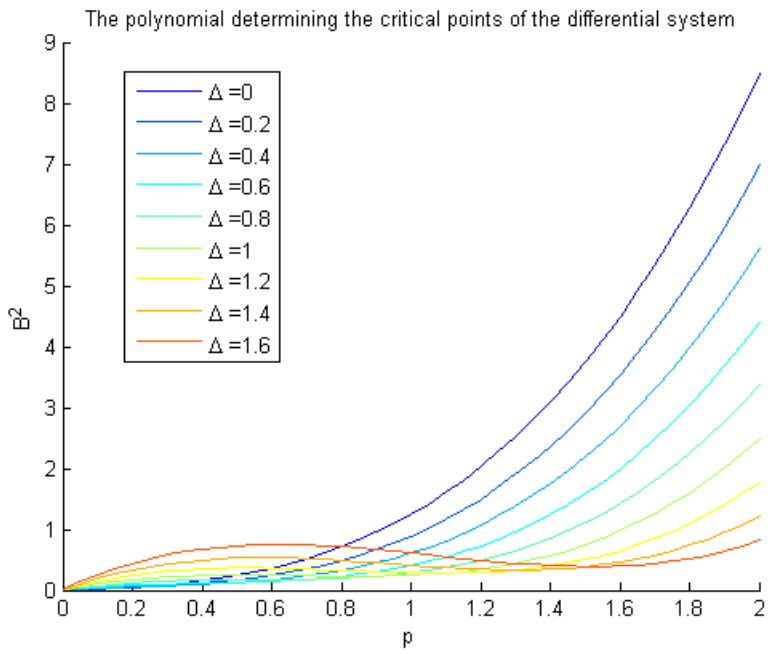

Figure 2: A plot of the polynomial determining $p = |A|^2$ as a function of $q^2 = |B|^2$ for several different values of Δ. Here we chose $d_1 = 1, Z = 1, \kappa = 1$.

Conversely we note that a critical point of the system is uniquely determined by its value of p, since this determines s and then also θ and x through the previous equations. We are interested in finding out if it is possible to have two or three solutions p satisfying the cubic equation given above, as a function of Δ and q. In order to answer this question we search for critical points of the system which are also critical points on the polynomial, i.e. points which satisfy:

$$\begin{aligned} 0 &= \frac{d}{dp}\left[d_1^2 p^3 - 2\Delta d_1 p^2 + \left(\frac{\kappa^2}{4} + \Delta^2\right) p - (qZ)^2\right] \\ &= 3d_1^2 p^2 - 4\Delta d_1 p + \left(\frac{\kappa^2}{4} + \Delta^2\right). \end{aligned}$$

The solutions of this quadratic equation are given by:

$$\begin{aligned} p_\pm &= \frac{1}{d_1}\frac{4\Delta \pm \sqrt{16\Delta^2 - 12\left(\frac{\kappa^2}{4} + \Delta^2\right)}}{6} \\ &= \frac{1}{d_1}\frac{2\Delta \pm \sqrt{\Delta^2 - \frac{3}{4}\kappa^2}}{3}. \end{aligned}$$

We note that if $|\Delta| < \frac{\kappa\sqrt{3}}{2}$ this equation has no real solutions. Furthermore, under the assumption that $\Delta^2 - \frac{3}{4}\kappa^2 \geq 0$, we note that $|2\Delta| > |\Delta| > \sqrt{\Delta^2 - \frac{3}{4}\kappa^2}$ (we get strict

inequality from the fact that $\kappa > 0$), so both solutions have the same sign. In particular, if $\Delta < 0$ then $p_\pm < 0$, which is not allowed, and if $\Delta > 0$ then $p_\pm > 0$. We conclude that if $\Delta < \frac{\kappa\sqrt{3}}{2}$ there are no critical points with $p > 0$, and if $\Delta > \frac{\kappa\sqrt{3}}{2}$ there are two such critical points. This means that, for fixed Δ, if $\Delta \leq \frac{\kappa\sqrt{3}}{2}$ for every q there is precisely one positive real solution p, and for $\Delta > \frac{\kappa\sqrt{3}}{2}$ there is a regime for q for which there are three solutions.

5.2 Stability

In the subsection below we will determine the stability of the critical points found in the previous section by linearising the system about a critical point. To do this we split A into a real and imaginary part: $A(t) = a(t) + ib(t)$ with a, b real. By introducing $v = \dot{x}$ and linearising the system of equations about a critical point (a_c, b_c, x_c) it follows that:

$$\begin{aligned}
\dot{x} &= v \\
\dot{v} &= -\Gamma_m v - \Omega_m^2 x + Y(2a_c a + 2b_c b) \\
\dot{a} &= -\frac{\kappa}{2}a - \left(\Delta - \omega_n \frac{x_c}{L}\right) b + \omega_n b_c \frac{x}{L} \\
\dot{b} &= \left(\Delta - \omega_n \frac{x_c}{L}\right) a - \frac{\kappa}{2}b - \omega_n a_c \frac{x}{L}
\end{aligned}$$

Introducing $\Delta_c = \Delta - \omega_n \frac{x_c}{L}$ allows us to rewrite the above to:

$$\frac{d}{dt}\begin{pmatrix} a \\ b \\ x \\ v \end{pmatrix} = \begin{pmatrix} -\frac{\kappa}{2} & -\Delta_c & b_c\frac{\omega_n}{L} & 0 \\ \Delta_c & -\frac{\kappa}{2} & -a_c\frac{\omega_n}{L} & 0 \\ 0 & 0 & 0 & 1 \\ 2Ya_c & 2Yb_c & -\Omega_m^2 & -\Gamma_m \end{pmatrix} \begin{pmatrix} a \\ b \\ x \\ v \end{pmatrix}.$$

Next we use the expression above to compute the characteristic polynomial:

$$
\begin{aligned}
P(\lambda) &= \begin{vmatrix} \lambda+\frac{\kappa}{2} & \Delta_c & -b_c\frac{\omega_n}{L} & 0 \\ -\Delta_c & \lambda+\frac{\kappa}{2} & a_c\frac{\omega_n}{L} & 0 \\ 0 & 0 & \lambda & -1 \\ -2Ya_c & -2Yb_c & \Omega_m^2 & \lambda+\Gamma_m \end{vmatrix} \\
&= \lambda(\lambda+\Gamma_m)\left(\left(\lambda+\frac{\kappa}{2}\right)^2+\Delta_c^2\right) - (-1)\begin{vmatrix} \lambda+\frac{\kappa}{2} & \Delta_c & -b_c\frac{\omega_n}{L} \\ -\Delta_c & \lambda+\frac{\kappa}{2} & a_c\frac{\omega_n}{L} \\ -2Ya_c & -2Yb_c & \Omega_m^2 \end{vmatrix} \\
&= \lambda(\lambda+\Gamma_m)\left(\left(\lambda+\frac{\kappa}{2}\right)^2+\Delta_c^2\right) + \left(\left(\lambda+\frac{\kappa}{2}\right)\left(\left(\lambda+\frac{\kappa}{2}\right)\Omega_m^2 + \frac{2a_cb_cY\omega_n}{L}\right)\right) \\
&- \Delta_c\left(-\Delta_c\Omega_m^2 + \frac{2a_c^2Y\omega_m}{L}\right) + \left(-b_c\frac{\omega_n}{L}\right)\left(2Yb_c\Delta_c + 2Ya_c\left(\lambda+\frac{\kappa}{2}\right)\right) \\
&= \lambda(\lambda+\Gamma_m)\left(\left(\lambda+\frac{\kappa}{2}\right)^2+\Delta_c^2\right) + \left(\lambda+\frac{\kappa}{2}\right)^2\Omega_m^2 + \Delta_c^2\Omega_m^2 \\
&- \Delta_c\frac{2Y\omega_n(a_c^2+b_c^2)}{L} \\
&= \lambda^4 + c_3\lambda^3 + c_2\lambda^2 + c_1\lambda + c_0
\end{aligned}
$$

We deduce the values of the constants c_0, c_1, c_2, c_3 from the expression above (by collecting terms). Expanding the last brackets gives us that:

$$
\begin{aligned}
c_3 &= \Gamma_m + \kappa \\
c_2 &= \kappa\Gamma_m + \frac{\kappa^2}{4} + \Delta_c^2 + \Omega_m^2 \\
c_1 &= \Gamma_m\left(\frac{\kappa^2}{4}+\Delta_c^2\right) + \kappa\Omega_m^2 \\
c_0 &= \Omega_m^2\left(\frac{\kappa^2}{4}+\Delta_c^2\right) - \Delta_c\frac{2Y\omega_n(a_c^2+b_c^2)}{L}
\end{aligned}
$$

Below we will draw some conclusions about the stability of the critical points by examining the characteristic polynomial above in more detail. Letting λ_i for $i = 1, \cdots, 4$ denote the eigenvalues around a critical point, we see that $\lambda_1\lambda_2\lambda_3\lambda_4 = c_0$ This follows from expanding the brackets in the equality $P(\lambda) = \prod_{i=1}^4(\lambda-\lambda_i) = \lambda^4 + c_3\lambda^3 + c_2\lambda^2 + c_1\lambda + c_0$.
Since P has real coefficients we know that if λ is an eigenvalue its complex conjugate is too. From this it follows that the sign of the product $\lambda_1\lambda_2\lambda_3\lambda_4$ is determined purely by the number of negative real roots of P. But since complex eigenvalues come in pairs we see that the number of real eigenvalues is even (as it is equal to 4 minus the number of non-real eigenvalues). In particular: if c_0 is negative we have an odd number of negative real eigenvalues, and therefore an odd number of positive real eigenvalues, and therefore

at least one positive real eigenvalue. So if $c_0 < 0$ at a critical point it is unstable. We next determine under which conditions this is the case:

$$0 > c_0 = \Omega_m^2 \left(\frac{\kappa^2}{4} + \Delta_c^2 \right) - \Delta_c \frac{2Y\omega_n(a_c^2 + b_c^2)}{L}.$$

We substitute $\Delta_c = \Delta - \omega_n \frac{x_c}{L}$, and note that, since (a_c, b_c, x_c) is a critical point of the system we know that $\Omega_m^2 x_c = Y(a_c^2 + b_c^2) = Yp$. By substituting this we get that the above equals:

$$c_0 = \Omega_m^2 \left(\frac{\kappa^2}{4} + \left(\Delta - \frac{\omega_n Y p}{\Omega_m^2 L} \right)^2 \right) - 2 \left(\Delta - \frac{\omega_n Y p}{\Omega_m^2 L} \right) \frac{2Y\omega_n p}{L}.$$

Substituting $d_1 = \left(\frac{\omega_n Y}{L\Omega_m^2} \right)$ from before allows us to rewrite this as:

$$\begin{aligned} c_0 &= \Omega_m^2 \left(\frac{\kappa^2}{4} + (\Delta - d_1 p)^2 \right) - 2(\Delta - d_1 p)\Omega_m^2 d_1 p \\ &= \Omega_m^2 \left[3d_1^2 p^2 - 4\Delta d_1 p + \left(\frac{\kappa^2}{4} + \Delta^2 \right) \right]. \end{aligned}$$

We recognise the equation between the square brackets as the equation we solved to find out if it were possible to have three critical points, and we immediately conclude that $c_0 < 0$ if $p_- < p < p_+$, so the downward slope of the cubic polynomial (see figure 2) consists of unstable critical points.

Also we note that c_3 is equal to minus the sum of the eigenvalues, i.e. $c_3 = -(\lambda_1 + \lambda_2 + \lambda_3 + \lambda_4)$. Since $c_3 = \Gamma_m + \kappa$ is strictly positive it follows that there must always be some stable direction (eigenvalue with negative real part). This insight will prove useful later. Unfortunately it is quite hard to determine the stabilities for values of p outside the range presented above. Since in those regimes c_0 is positive we know that the number of stable directions is even (this follows from an argument similar to the one above), and we have just shown that there is at least one stable direction. Unfortunately it is not easy to see if there are 4 stable directions, in which case the critical point is stable, or if there are 2 stable directions and 2 unstable directions.

Using numerical approximations we can compute the eigenvalues of the critical point for close $|B|^2$, and we find that all four eigenvalues have negative real part. Therefore we expect the rising slope before the bistable regime to be stable.

5.3 Chaos

In the previous subsection we have looked for critical points where one of the eigenvalues is equal to 0. In this subsection we will look for Hopf bifurcations, characterized by a purely imaginary (non-zero) eigenvalue.

Our interest in Hopf bifurcations is twofold. Firstly we know that bifurcations occur when the sign of the real part of one or more eigenvalues of the system changes. In the previous subsection we have looked for critical points satisfying $c_0 = 0$, i.e. $\lambda_i = 0$ for some i (this follows again from the fact that $P(\lambda) = \prod_{i=1}^{4}(\lambda - \lambda_i) = \lambda^4 + c_3\lambda^3 + c_2\lambda^2 + c_1\lambda + c_0$ so $c_0 = \lambda_1\lambda_2\lambda_3\lambda_4$). The only other possibility for an eigenvalue to change sign of real part is when it becomes purely imaginary, and bifurcations of this type are the Hopf bifurcations. So through looking for these will have completely mapped the bifurcation diagram.
Secondly we are interested in Hopf bifurcations since in systems with at least three dimensions (our system is 4-dimensional) a Hopf bifurcation is often an indicator of chaotic behaviour, which is of great interest to experiments.

To locate the Hopf bifurcations we set $\lambda = i\nu$ where $\nu \in \mathbb{R}_{>0}$. We can demand that $\nu > 0$ since $\bar{\lambda} = -i\nu$ is another eigenvalue of the system as the characteristic polynomial is real. Substituting this in our characteristic polynomial yields:

$$0 = \nu^4 - ic_3\nu^3 - c_2\nu^2 + ic_1\nu + c_0.$$

We now find the following equalities from collecting real and imaginary parts:

$$\begin{aligned} 0 &= \nu^4 - c_2\nu^2 + c_0. \\ 0 &= -c_3\nu^3 + c_1\nu. \end{aligned}$$

From the second equation it follows that:

$$\nu = \sqrt{\frac{c_1}{c_3}}.$$

Note that c_1 and c_3 are positive for all values of Δ_c and x_c, so this root exists. We can substitute this equality in our other equation to get:

$$0 = \left(\frac{c_1}{c_3}\right)^2 - c_2\left(\frac{c_1}{c_3}\right) + c_0.$$

We now rearrange terms to get:

$$c_0 = \frac{c_1}{c_3^2}(c_2c_3 - c_1).$$

Below is an image of this curve as a function of Δ_c and $\frac{x_c}{L}$:

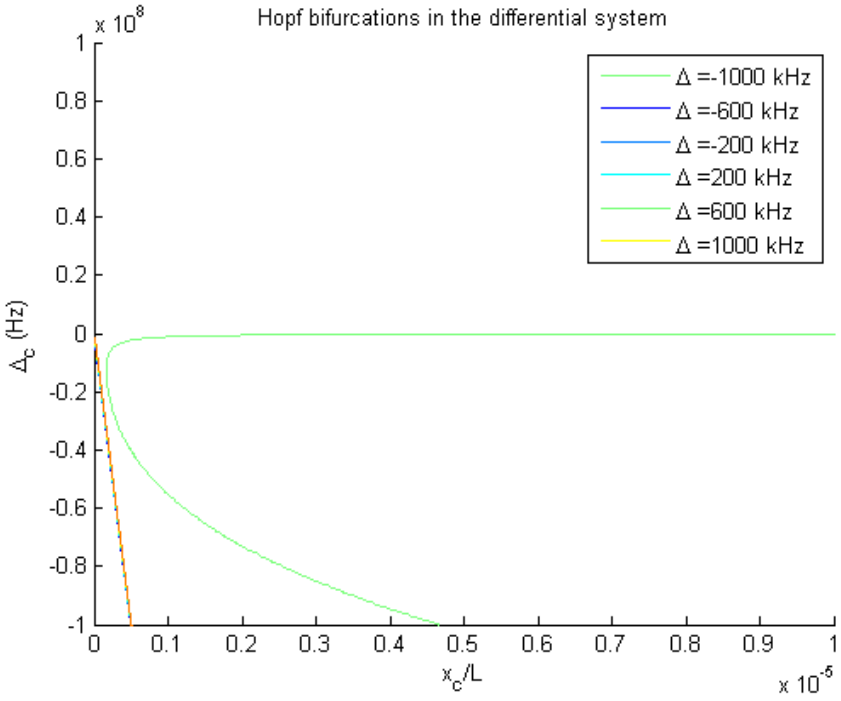

Figure 3: A plot of the curve $c_1^2 - c_1c_2c_3 + c_0c_3^2 = 0$. Here $\Gamma_m = 10^3$ s^{-1}, $\Omega_m = 10^5$ Hz, $\omega_n = 2 \cdot 10^{14}$ Hz and κ is determined by $\alpha = 0, \tau(t) = \tau_c, L = 10$ cm and $r_1 = r_2 = 0.99$. Also plotted are some lines with constant Δ, indistinguishable at this scale.

Note that $x_c > 0$ since $x_c\Omega_m^2 = Y|A_c|^2$. From this we see in the figure that, for these values of the constants involved, the Hopf bifurcations only occur for $\Delta_c < 0$. This no longer holds if we change the values of some of the parameters - below is a plot of the same curve where we have changed κ by setting $r_1 = r_2 = 0.995$:

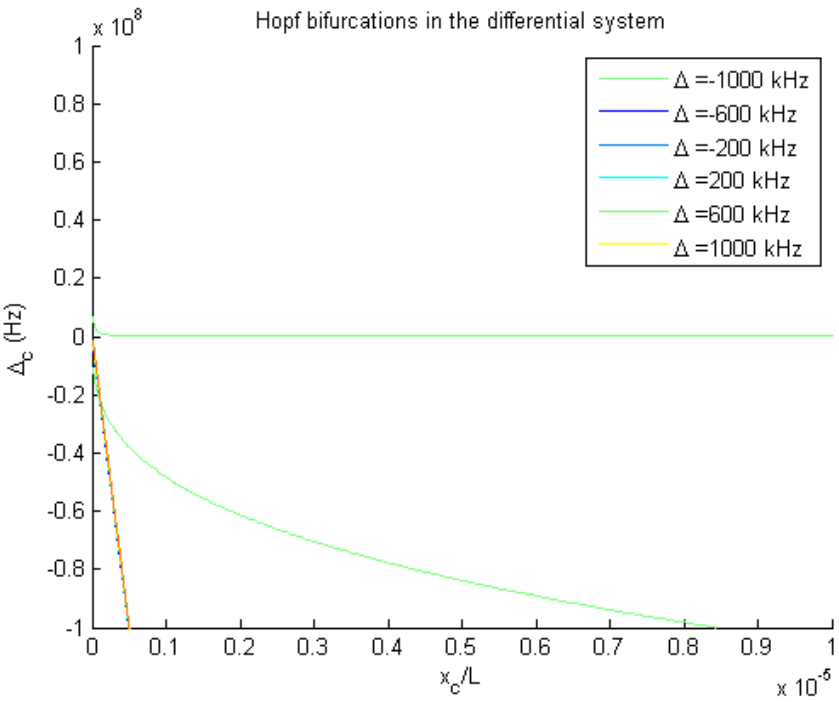

Figure 4: A plot of the curve $c_1^2 - c_1 c_2 c_3 + c_0 c_3^2 = 0$. Here $\Gamma_m = 10^3$ s^{-1}, $\Omega_m = 10^5$ Hz, $\omega_n = 2 \cdot 10^{14}$ Hz and κ is determined by $\alpha = 0, \tau(t) = \tau_c, L = 10$ cm and $r_1 = r_2 = 0.995$. Also plotted are some lines with constant Δ, indistinguishable at this scale.

Actually we are not completely interested in the locations of the Hopf Bifurcations as a function of x_c and Δ_c - we only adopted these variables as bifurcation variables to simplify the calculations. Really we are interested in the locations of the Hopf bifurcations as a function of Δ and q, or Δ and x_c. Plotted in both figures are some lines with Δ constant, over a typically large range of values for Δ. In figure 4 all the lines intersect the Hopf curve around $\frac{x_c}{L} = 1.1 \cdot 10^{-7}$, or $x_c \approx 11$ nm. In figure 3 the lines do not intersect the Hopf curve at all. We conclude that the critical value of x_c of the location of the Hopf bifurcation, which depends only weakly on Δ, is very sensitive with respect to κ. It is therefore hard to say what the maximum admissible input power $|B|^2$ is at which the critical point we found is still stable.

6 Numerical results

In this section we numerically explore the behaviour of the different systems introduced in the previous chapters. We will look at three different simulations: firstly a simulation showing (approximations of) the solutions to the difference and the differential system. Secondly a simulation that resembles the conditions of the physical measurement, where we have manually set $x(t)$ to be equal to a sine function with known amplitude and frequency, so $x(t) = a\sin(\Omega t)$. In this simulation $x(t)$ will not satisfy equation 1, so we restrict our model to just equation 3. We are interested the power of the transmission and reflection, which can be computed easily from $A(t)$. Lastly we will simulate the behaviour of $A(t)$ and $x(t)$ in the bistable regime of the differential system. For the experimentally relevant simulation we will only concern ourselves with the differential system. The reason for this is that in order to accurately simulate the system with the difference equation we need a very small timestep, and in order to calculate results over timescales which can actually be measured we then need a tremendous number of points, so the simulations take too long. Also, as we can see in subsection 6.1, we expect the two systems to be in good agreement.

6.1 Comparison between systems

Below we have plotted in the same graphs numerical approximations of the solutions to the difference and the differential system. As initial values we set $A(t) = 0, x(t) = 0$ for all $t \leq 0$. We have set $\alpha = 0$ and determined κ by substituting $\tau(t) \approx \frac{2L}{c}$ in the following equation:

$$\kappa(t) = 2\left(\alpha c - \frac{1}{\tau(t)}\log(r_1 r_2)\right)$$

Here we have set $r_1 = r_2 = -\sqrt{0.9994}$, and $T_1 = T_2 = 1 - r_1^2 = 1 - r_2^2 = 0.0006$. Furthermore we have set $L = 10$ cm, $\omega = \frac{2\pi c}{1064\text{ nm}}$, $B^2 = 365\mu$W, $\Omega_m = 150$ kHz, $\Gamma_m = 150$ kHz, $m_{\text{eff}} = 50$ g and $\Delta = 0$ Hz. These values correspond to the values in the actual experiment. From this we find:

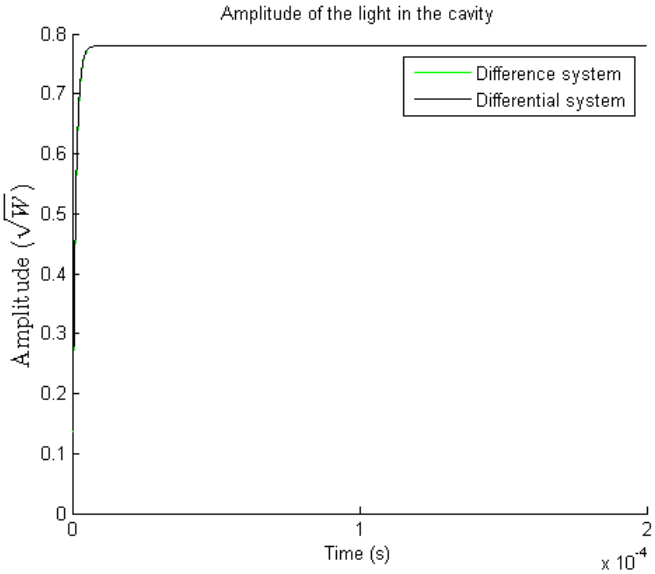

Figure 5: Amplitude of the light in the cavity, $|A|$, computed with the two different systems of equations describing the experiment.

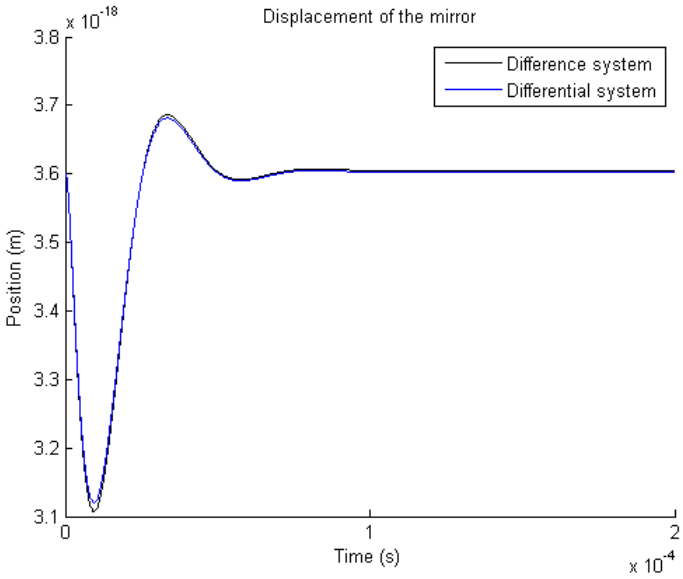

Figure 6: Displacement of the mirror, x, computed with the two different systems of equations describing the experiment.

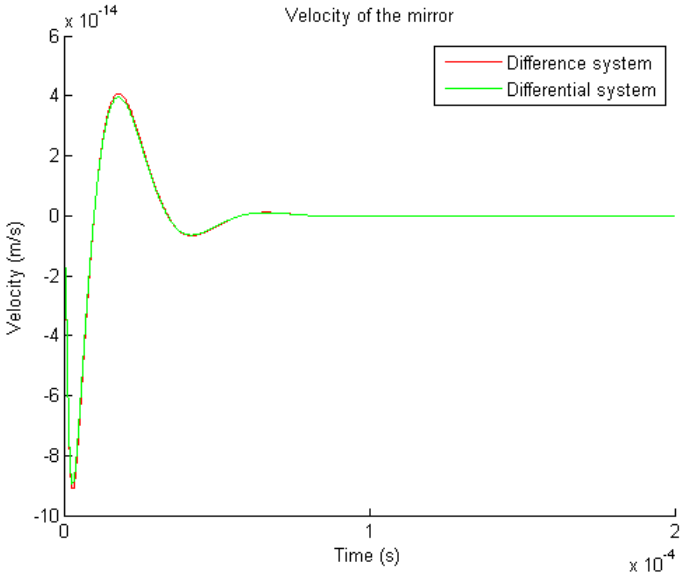

Figure 7: Velocity of the mirror, v, computed with the two different systems of equations describing the experiment.

We note that the two approximations are in good agreement, the amplitudes of the light agree to within 0.5%, the positions differ by only up to 2% (note: since the position has an offset this percentage has been determined by dividing the maximal difference between the two graphs by the peak-to-peak length of the graphs) and the velocities coincide to within 1%.

6.2 Driven oscillation

In this simulation we will fix $x(t)$ to be equal to $x(t) = a\sin(\Omega t)$, and from this we compute the power of the reflection and transmission from the cavity, which is the light escaping the cavity in the direction of the source. At the outer surface of the fixed mirror we can write the amplitude of the field as a sum of the light that escaped the cavity and the light from the source that has just reflected off the outer surface of the fixed mirror. From this we find that the power of the reflected light can be approximated with $\left|r_2 t_1 \mathcal{A}\left(t - \frac{L}{c}\right) + r_1 B e^{-i\omega t}\right|^2$. This is only an approximation, as actually the complex amplitude of the light at the cavity at time t equals the sum of the source contribution at time t, multiplied by r_1 as it gets reflected on the outer mirror, plus a contribution from inside the cavity. However, the light that left the surface of the moving mirror at a time t_0 can contribute to this reflection term only at time $t_0 + \frac{L+x(t_0)}{c}$, so we need to find a $t_0(t)$ such that this is equal to t. Since $|x| \ll L$ we can approximate the expression above with $t_0 + \frac{L}{c}$ to find $t_0(t) = t - \frac{L}{c}$, and we derive the formula presented above for the power of the reflected beam. The power of the transmitted beam is simply given by $|t_2\mathcal{A}(t)|^2$.
We have simulated this reflection and transmission intensity for different values of Ω, we have picked $\Omega = 50$ kHz en $\Omega = 212.7$ kHz, as these are some of the frequencies we have measured at. Here we used $\Omega_m = 150$ kHz, $\Gamma_m = 150$ kHz. These values roughly correspond to the values from the actual setup, although more commonly we have $Q_m = \frac{\Omega_m}{\Gamma_m} \gg 1$. For both simulations we have set $a = 1.5$ nm. Furthermore we have picked most of our other values equal to those in the other simulation; $L = 10$ cm, $r_1 = r_2 = -\sqrt{0.9994}$, $T_1 = T_2 = 1 - r_1^2 = 1 - r_2^2 = 0.0006$, $B^2 = 365\mu$W and $\omega = \frac{2\pi c}{1064\text{ nm}}$. This time however we also had a detuning of $\Delta = -1$ MHz. We included this detuning since in the actual experiment we fix the laser frequency to (a fix-point on) the slope of the transmission peak, rather than the top of this peak. Below we present the results of the simulations:

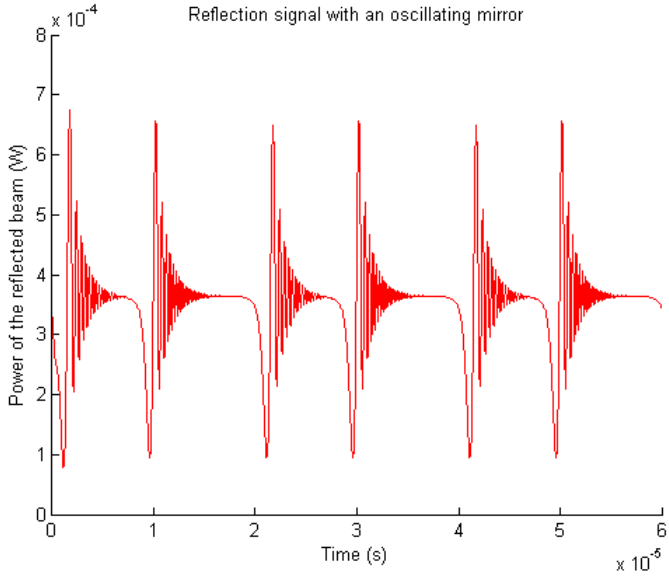

Figure 8: Power of the reflected beam (derived from $A(t)$ using the formulas presented above) when we force the piezo to oscillate at 50 kHz.

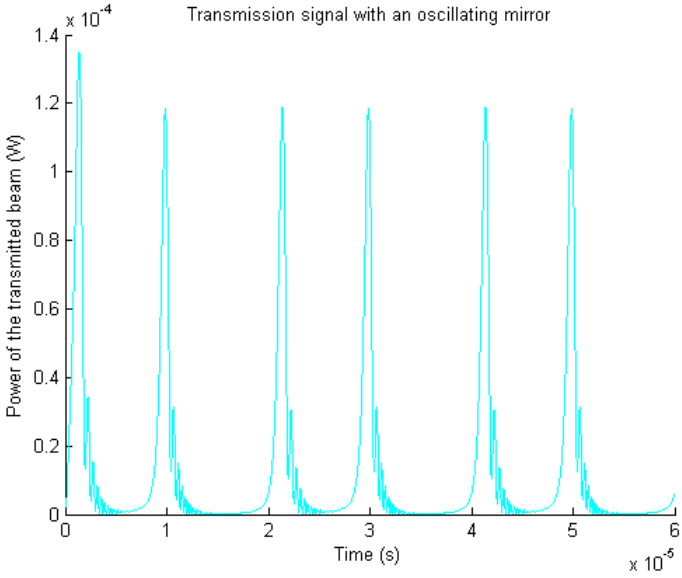

Figure 9: Power of the transmitted beam (derived from $A(t)$ using the formulas presented above) when we force the piezo to oscillate at 50 kHz.

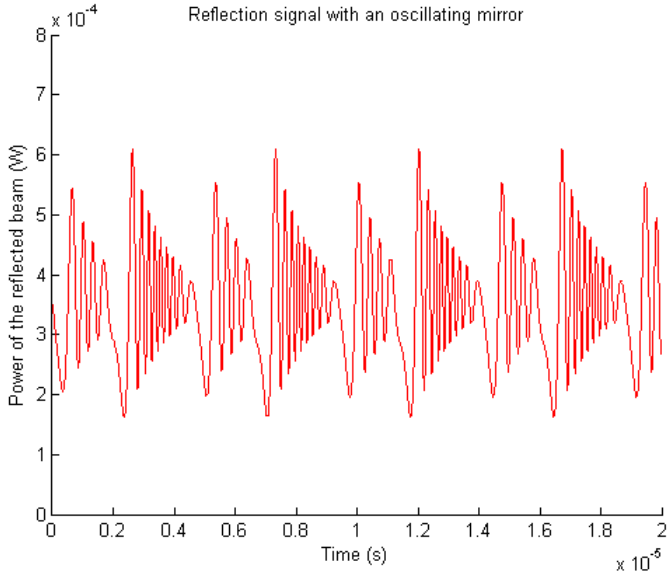

Figure 10: Power of the reflected beam (derived from $A(t)$ using the formulas presented above) when we force the piezo to oscillate at 212.7 kHz.

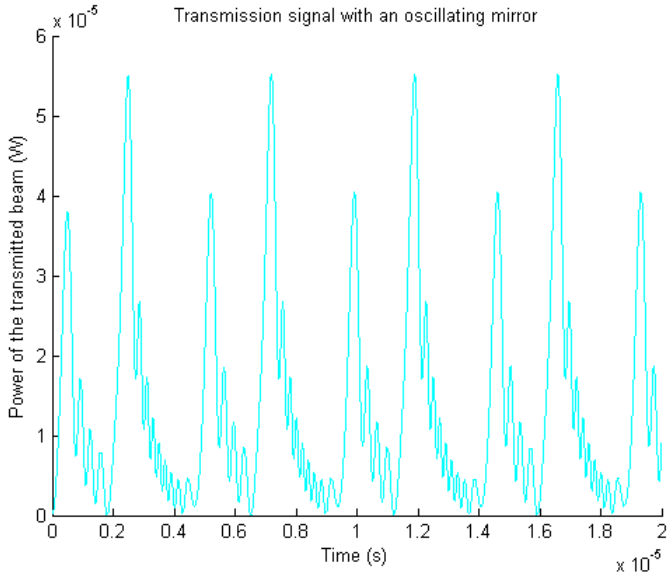

Figure 11: Power of the transmitted beam (derived from $A(t)$ using the formulas presented above) when we force the piezo to oscillate at 212.7 kHz.

It is interesting to note that the power of the reflection differs by up to 80% in both directions from the power of the input beam, which is 365μW, while the oscillation of the mirror has a peak-to-peak amplitude of only 3 nm, which is small compared to the wavelength $\lambda = 1064$ nm.

6.3 Bistable regime

In this subsection we will present a simulation in the bistable regime of the differential system. The mirror is therefore not driven in this simulation. We have picked most values similar to those in the previous sections - we have set $r_1 = r_2 = -\sqrt{0.9994}$ and $T_1 = T_2 = 1 - r_1^2 = 1 - r_2^2 = 0.0006$. Furthermore we have set $L = 10$ cm, $\omega = \frac{2\pi c}{1064 \text{ nm}}$, $\Omega_m = 150$ kHz, $\Gamma_m = 150$ kHz and $m_{\text{eff}} = 50$ g. Furthermore we have chosen the initial conditions $A(t) = 0, x(t) = 0$ for $x \leq 0$. Also we have set $\Delta = 2\kappa$, so $\Delta > \frac{\kappa\sqrt{3}}{2}$, and we have set $B^2 = \frac{2\Delta}{3d_1}$ so $p_- < B^2 < p_+$. The results of the simulations are shown below:

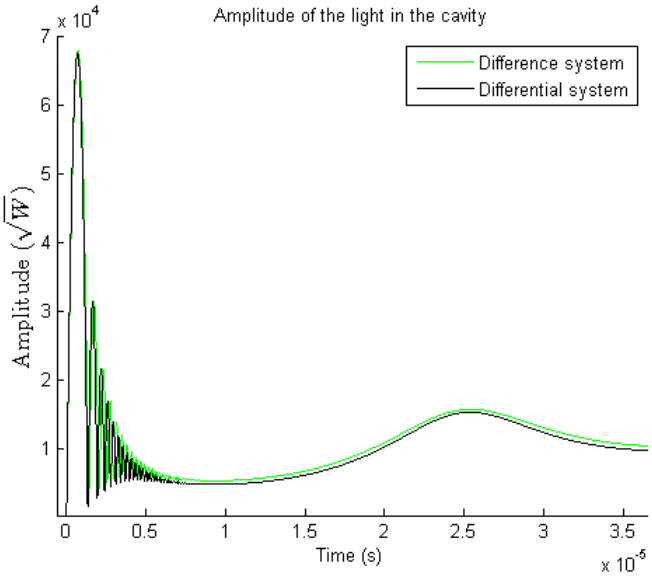

Figure 12: Amplitude of the light in the cavity, $|A|$, computed with the two different systems of equations describing the experiment. The parameters were chosen such that the differential system is bistable.

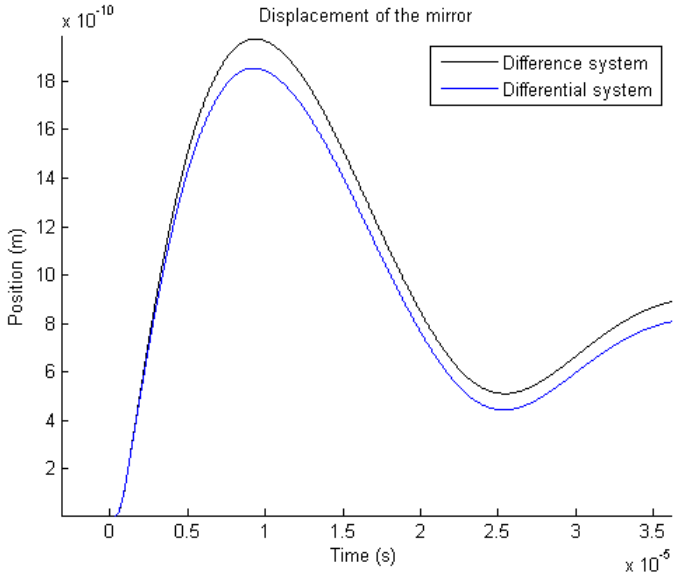

Figure 13: Displacement of the mirror, x, computed with the two different systems of equations describing the experiment. The parameters were chosen such that the differential system is bistable.

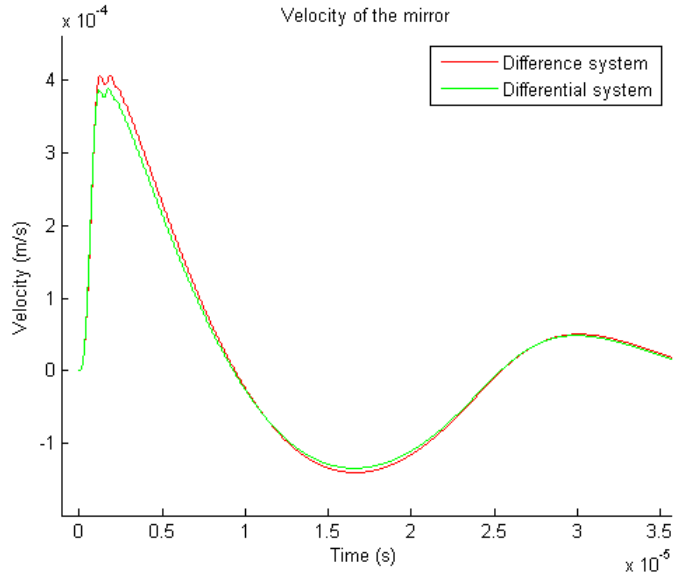

Figure 14: Velocity of the mirror, v, computed with the two different systems of equations describing the experiment. The parameters were chosen such that the differential system is bistable.

Interesting to note are the oscillations at the peak of the velocity around $t = 0.2 \cdot 10^{-6}$ s and the oscillations at the downward slope in the amplitude of the light in the cavity for $0.3 \cdot 10^{-6}$ s $< t < 0.6 \cdot 10^{-6}$ s. Also worthy of note is that the two systems are not in great agreement - the solutions are quite similar, but the differences are notable.
Lastly it should be mentioned that, using the values mentioned above, we find an input power of $B^2 = 2.29 \cdot 10^7$ W, which is unreachable in practice.

7 Materials and Methods

Below we present present the layout of the experiment and supply details of the equipment used in the setup. Also we explain what we will measure, and how we will measure this with our setup.

7.1 Materials

A schematic representation of the setup is presented in figure 15:

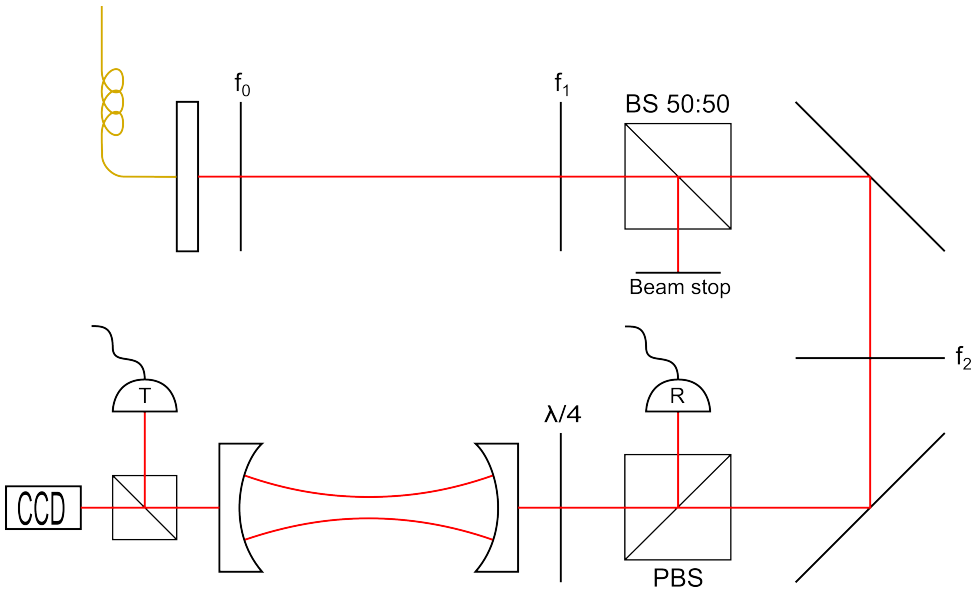

Figure 15: A schematic overview of the setup used in the experiment.

For the source we use a single-mode fibre transferring light from a laser from another setup. Specifications of the laser can be found below. We use several windings of the fibre to match the polarisation of the emitted light with the orientation of the polarising beam splitter further on in the setup. To improve the mode-matching to the cavity modes (see appendix B) we placed a telescope directly after the end of the fibre. Next we split the beam (50:50), the reflection arm is to be used in a second experiment. After this we place a periscope, as well as an extra lens, to increase the coupling to the cavity modes (see appendix B). Using a polarising beam splitter and a quarter wave plate we can measure the reflection from the cavity. The polarising beam splitter only transmits light with a vertical polarisation, which is the polarisation of the incoming beam. Light reflected on the cavity and coming back to the PBS passes the quarter wave plate twice. On the first passing the linearly polarised light becomes circularly polarised. The direction of polarisation is next inverted upon reflection at the mirror, and then transformed to a linear polarisation at the quarter wave plate again, now with a horizontal polarisation. This is next reflected on the

PBS and sent to the detector.
After this we have placed the cavity, of which the specifications are given below. After the cavity is a beam splitter, dividing the light between a CCD camera and a detector.
The power of the beam emitted from the fibre end is $807\mu W \pm 2\mu W$, of which $365\mu W \pm 10\mu W$ arrived at the cavity.

Source

Light from the laser is transferred by a single-mode fibre. The end of this fibre is fitted in a Thorlabs TC12APC-1064 triplet collimator to collimate the beam. However, it is still divergent in our setup. The laser we used is a Toptica DLpro tunable laser operating at 1064 nm with a linewidth of 150 kHz. We scan the laser over 1.5 Ghz, the free spectral range of the cavity, to find the fundamental mode of the cavity, after which we lock the laser frequency to a set-point on the rising slope of the transmission peak.

Cavity

The cavity we use consists of two concave mirrors with a radius of curvature of 50 cm and a power reflection coefficient of $R = 99.94\% \pm 0.01\%$. The distance between these two mirrors is 10 cm. Both mirrors are equipped with a piezoelectric element (piezo) which we can use to modify the distance between the mirrors. We have measured the response (in nm/V) of the piezo's at different frequencies with the use of a wave generator, the results of which are presented in table 1. We have determined the displacement of the large piezo with interferometry on the reflection (using a 1550 nm laser source). The response of the small piezo was determined by slowly scanning the laser frequency and detecting the width of the detection peak, from which we can derive the amplitude of the movement of the mirror. We use this measured response later to set the amplitude of the oscillation of the piezo. We have therefore measured the response at many different frequencies, rather than measure a few and extrapolate. Lastly we have determined the finesse of the cavity, which is a measure of the number of round trips a photon makes in the cavity before being transmitted, to be 2500 ± 300. The finesse of a cavity can be determined in several ways. We measured the free spectral range and the linewidth of the fundamental mode (full width half height), the finesse is equal to their ratio.

Detectors

The photo-detector used for measuring the intensity of the reflection is a APD110C/M Thorlabs avalanche photo-detector. At a gain of 3dB the bandwidth of this detector is 50 MHz.
For the transmission measurements we used a PDA36A-EC Thorlabs Si switchable gain detector. During our measurements the gain was set at 60dB since the signal was not distinguishable at lower gain. At this gain setting the detector has a bandwidth of 11 kHz, which is lower than some of the frequencies we measured at. The transmission data was therefore only used for the laser locking (see subsection 7.2).

Table 1: Response of the piezo's at different driving frequencies. All measurements on the small piezo have an error of ±0.02 nm/V, all measurements on the large piezo have an error of ±1 nm/V.

f (Hz)	Response of front (large) piezo (nm/V)	Response of back (small) piezo (nm/V)
10	–	0.26
20	–	0.24
90	–	0.25
100	3	–
210	–	0.26
250	3	–
520	–	0.26
1k	3	0.27
2k	–	0.27
4k	1.2	–
5k	–	0.28
10k	–	0.30
50k	–	0.20
100k	–	0.17
200k	–	0.07
212.7k	–	0.13
300k	–	0.11
600k	–	0.07
602.5k	–	0.11
800k	–	0.13

7.2 Method

In the experiment we send the detected signal at the transmission detector back to a PI-loop regulating the frequency of the laser, fixing the height of the transmission signal. This counteracts changes in the signal caused by slow movements of the cavity. After having locked the laser we drive the piezo element at a frequency too fast for the PI-feedback to handle, so the feedback loop will lock on the average of many periods of the moving piezo rather than the instant signal. We detect the reflection intensity, transmission intensity and the feedback sent to the laser, and compute a Fourier transform. From this Fourier transform we discard all data except for a small region around each integer multiple of the driving frequency (we kept all data within 10 Hz from the resonance frequency and its multiples and discarded the rest). From this reduced data we can reconstruct how the light responds to the oscillating piezo.
Since we used the transmission measurement, which has a bandwidth of only 11 kHz, to lock the laser to the cavity we can use this method for frequencies higher than 11 kHz.
For the data acquisition we use a DAQmx card, which can only measure at a rate of 1.25 MHz single-channel or 500 kHz with three channels. Since we are interested in high harmonics of the driving frequency we will restrict ourselves to measuring a single channel. The reflection data and data from the feedback are therefore not acquired at the same moment.

8 Results

We have observed several of the spatial modes supported by our cavity (more on mode-matching is presented in appendix B), as shown below:

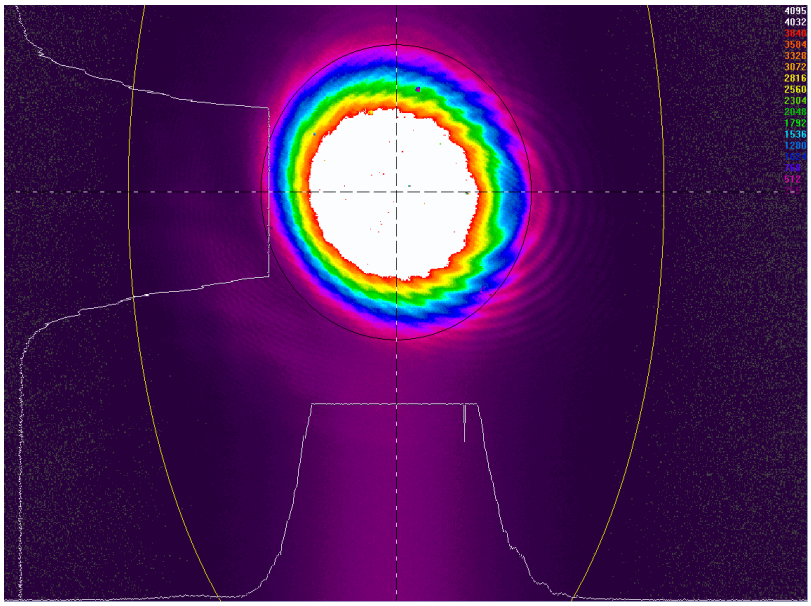

Figure 16: An image made with the CCD located in the transmission arm of the setup. Here we have tuned the frequency of the laser to couple primarily into the (fundamental) TEM_{00} mode.

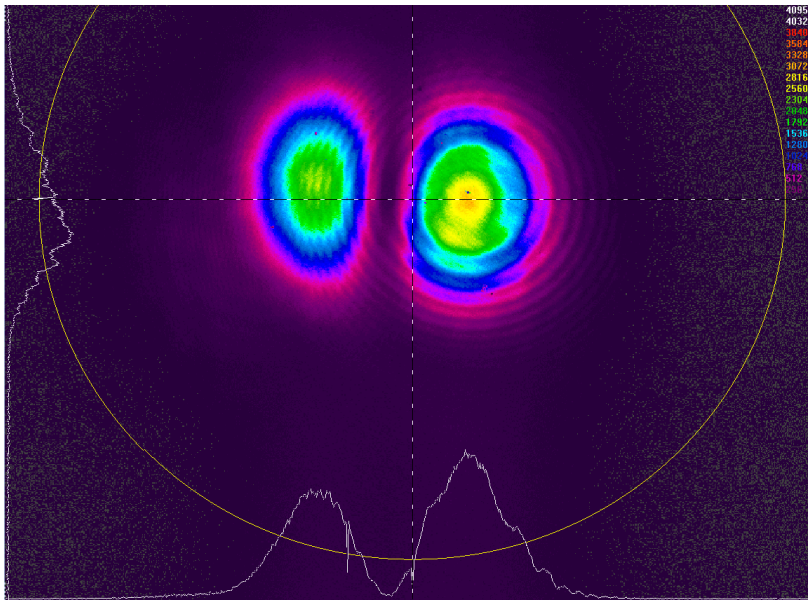

Figure 17: An image made with the CCD located in the transmission arm of the setup. Here we have tuned the frequency of the laser to couple primarily into the TEM_{01} mode.

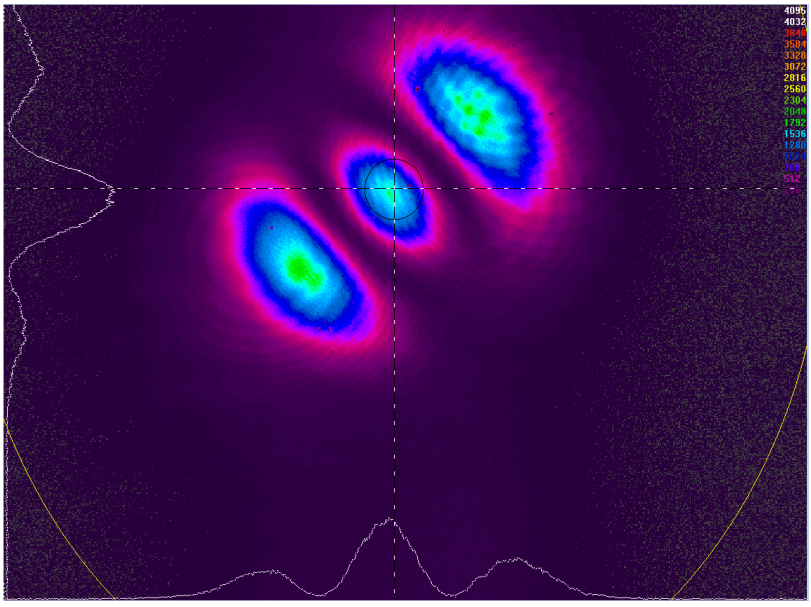

Figure 18: An image made with the CCD located in the transmission arm of the setup. Here we have tuned the frequency of the laser to couple primarily into the TEM_{02} mode.

Below we will present the data acquired using the method and setup described in chapter 7. We have measured the reflection as well as the feedback signal from the PI at driving frequencies of 10 kHz, 50 kHz, 200 kHz and 212.7 kHz. In section 9 we will present arguments for these particular choices of frequencies. The results of these measurements can be seen below.

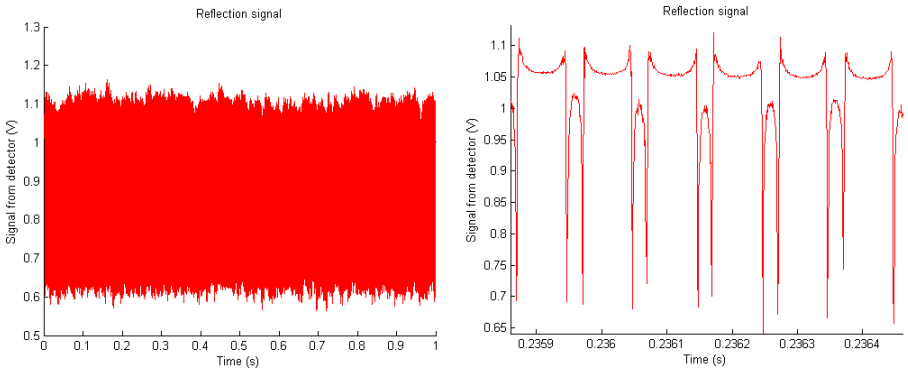

Figure 19: The left graph is the signal (in Volt) of the detector in the reflection arm of the setup while the small piezo (backmost mirror) was oscillating with a sine wave with a frequency of 10 kHz and an amplitude of 3 nm (6 nmpp). The picture on the right is a closer zoom of the one on the left.

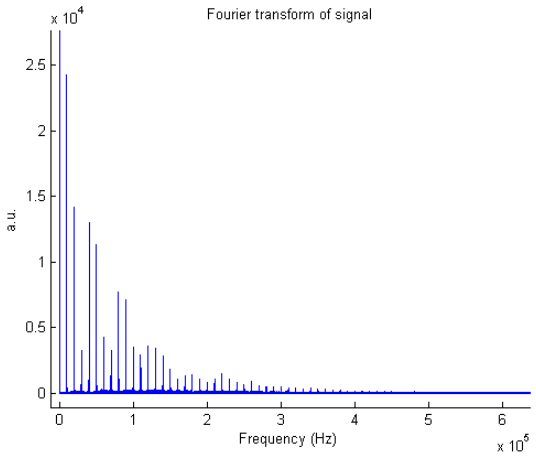

Figure 20: The Fourier transform of the measurement above, where the piezo element was oscillating with a sine wave with a frequency of 10 kHz and an amplitude of 3 nm (6 nmpp). We have rescaled the vertical axis to be able to see the peaks (the DC component is dominating the signal).

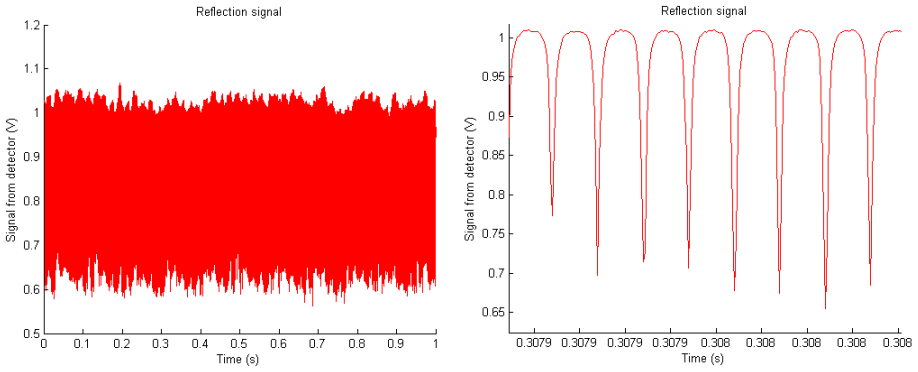

Figure 21: The left graph is the signal (in Volt) of the detector in the reflection arm of the setup while the small piezo (backmost mirror) was oscillating with a sine wave with a frequency of 50 kHz and an amplitude of 1.5 nm (3 nmpp). The picture on the right is a closer zoom of the one on the left.

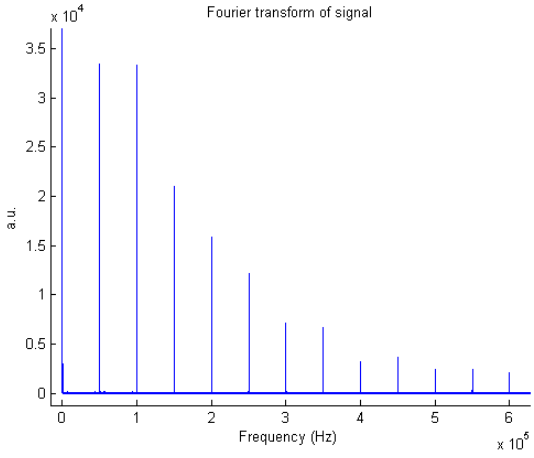

Figure 22: The Fourier transform of the measurement above, where the piezo element was oscillating with a sine wave with a frequency of 50 kHz and an amplitude of 1.5 nm (3 nmpp). We have rescaled the vertical axis to be able to see the peaks (the DC component is dominating the signal).

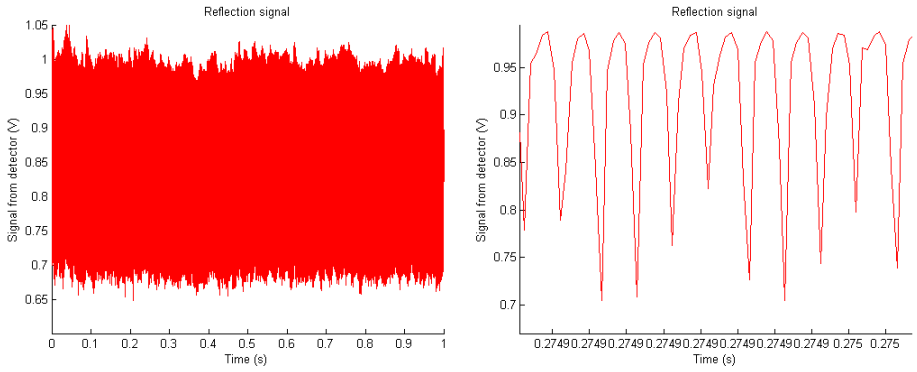

Figure 23: The left graph is the signal (in Volt) of the detector in the reflection arm of the setup while the small piezo (backmost mirror) was oscillating with a sine wave with a frequency of 200 kHz and an amplitude of 1.5 nm (3 nmpp). The picture on the right is a closer zoom of the one on the left.

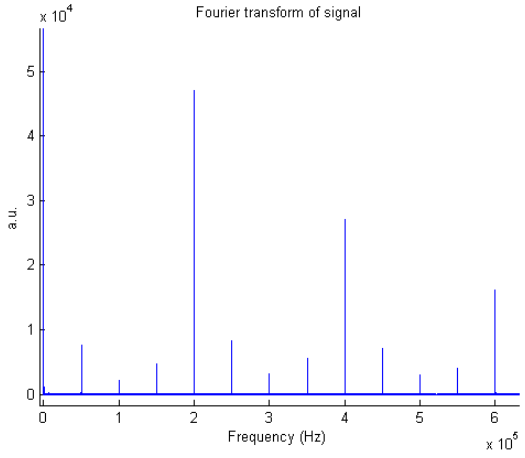

Figure 24: The Fourier transform of the measurement above, where the piezo element was oscillating with a sine wave with a frequency of 200 kHz and an amplitude of 1.5 nm (3 nmpp). We have rescaled the vertical axis to be able to see the peaks (the DC component is dominating the signal).

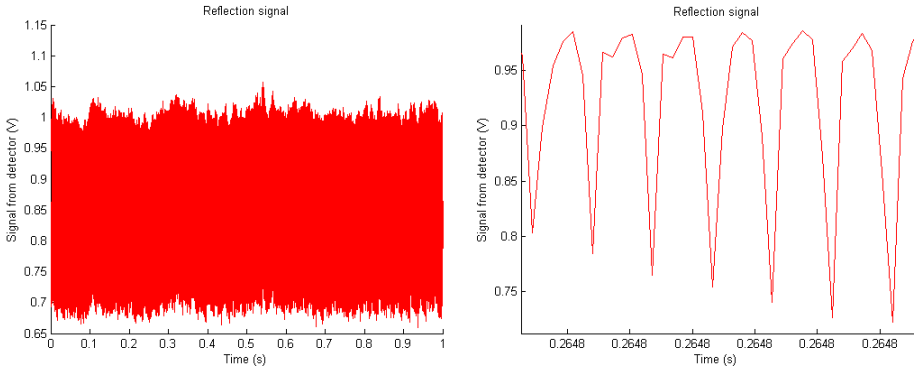

Figure 25: The left graph is the signal (in Volt) of the detector in the reflection arm of the setup while the small piezo (backmost mirror) was oscillating with a sine wave with a frequency of 212.7 kHz and an amplitude of 1.5 nm (3 nmpp). The picture on the right is a closer zoom of the one on the left.

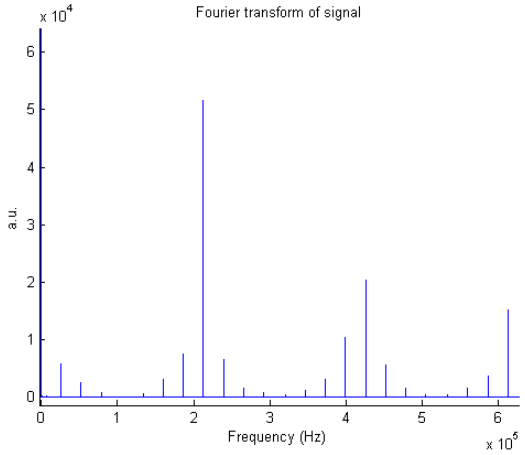

Figure 26: The Fourier transform of the measurement above, where the piezo element was oscillating with a sine wave with a frequency of 212.7 kHz and an amplitude of 1.5 nm (3 nmpp). We have rescaled the vertical axis to be able to see the peaks (the DC component is dominating the signal).

As mentioned we have also recorded the signal of the PI-loop locking the laser, the results of which are shown below:

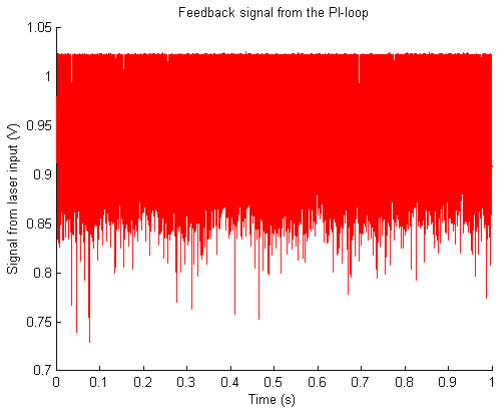

Figure 27: Feedback signal to the laser while the piezo is oscillating with a sine wave with a frequency of 10 kHz and an amplitude of 3 nm (6 nmpp).

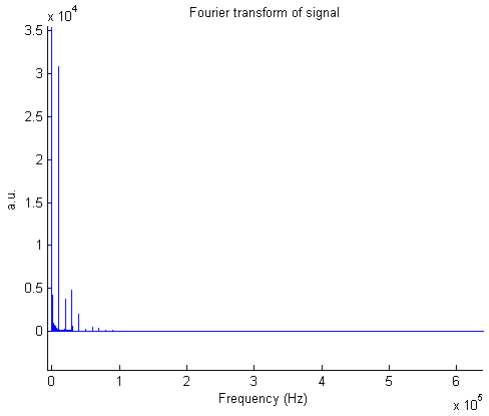

Figure 28: Fourier transform of the feedback signal to the laser while the piezo is oscillating with a sine wave with a frequency of 10 kHz and an amplitude of 3 nm (6 nmpp).

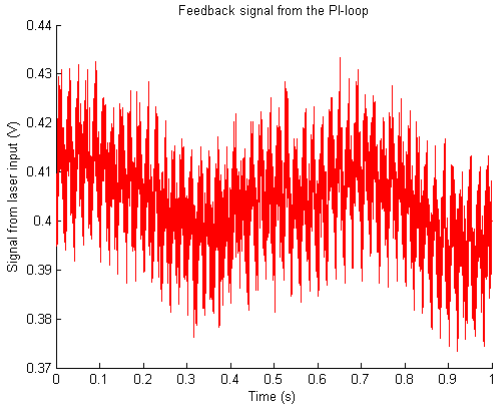

Figure 29: Feedback signal to the laser while the piezo is oscillating with a sine wave with a frequency of 50 kHz and an amplitude of 1.5 nm (3 nmpp).

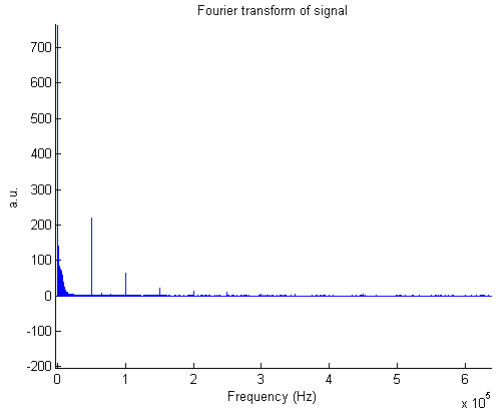

Figure 30: Fourier transform of the feedback signal to the laser while the piezo is oscillating with a sine wave with a frequency of 50 kHz and an amplitude of 1.5 nm (3 nmpp).

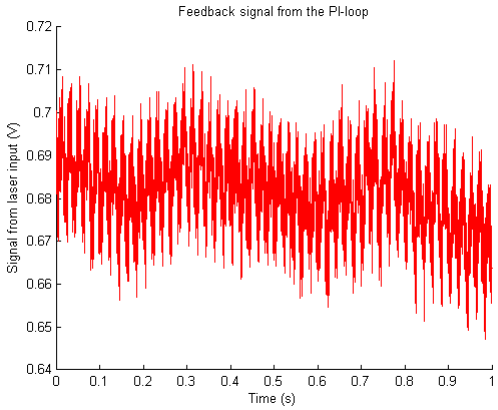

Figure 31: Feedback signal to the laser while the piezo is oscillating with a sine wave with a frequency of 200 kHz and an amplitude of 1.5 nm (3 nmpp).

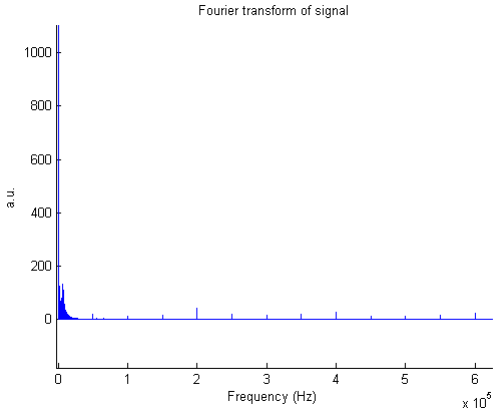

Figure 32: Fourier transform of the feedback signal to the laser while the piezo is oscillating with a sine wave with a frequency of 200 kHz and an amplitude of 1.5 nm (3 nmpp).

9 Discussion

In this section we will interpret the data and compare it to our simulations and theory. Also we will look more closely at the method used to isolate the relevant data from the measurements. Lastly we will present possible explanations for any discrepancies between the data and the models, and highlight experimental obstacles that increased the measurement difficulty.

The graph that needs our immediate attention is figure 27, the PI feedback signal to the laser at a driving frequency of 10 kHz. We see that the feedback signal to lock the laser jumps between a noisy lower level and a relatively fixed upper level, and if we zoom in on the picture (as shown in figure 33) we see that the transition between the two levels contains an oscillation at the driving frequency of 10 kHz (as the minima are often 0.1 ms apart).

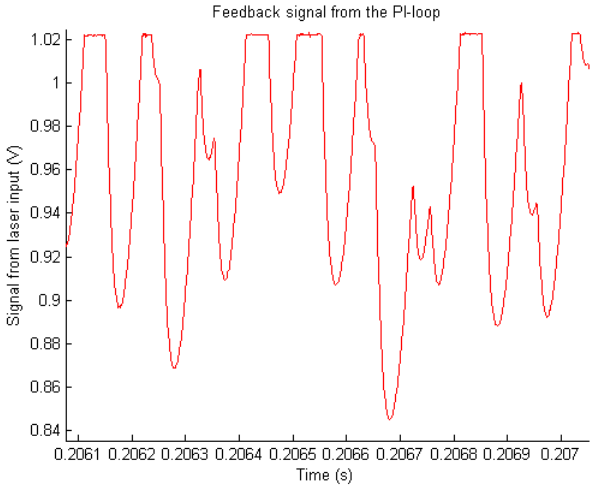

Figure 33: Feedback signal to the laser while the piezo is oscillating with a sine wave with a frequency of 10 kHz and an amplitude of 3 nm (6 nmpp). We have zoomed in to make oscillations on timescales of the order of 0.1 ms more visible

Presumably the lock of the laser to the cavity is not stable, and the feedback signal jumps back and forth between a locked state (the noisy lower level) and an unlocked out-of-bound state (the fixed upper level), which may give rise to strange components in the Fourier spectrum of the transmission and reflection signal. It seems that the driving frequency of the piezo was too low to make the PI loop average over many periods, so our method did not work at this frequency.

However, we can still draw some conclusions based on the data presented above. We expect that the PI-loop, regulating the laser, will mainly reduce fluctuations in the signal

rather than enhance them. Therefore any peaks (other than the DC peak) in the Fourier spectrum of the reflection signal (figure 20) have only been decreased by the improper lock, and we can use the amount of discernible peaks as an estimate for the number of higher harmonics present in the signal that we would see with a proper lock.
Upon inspection we see around 40 higher harmonics clearly distinguishable from noise, so we conclude that with a proper lock the signal should have many overtones and fluctuates on small timescales.

We now look at the feedback data at a driving frequency of 50 kHz, shown in figure 29. From an analysis of the Fourier transform of this signal, shown in figure 30, we see that the feedback signal consists almost entirely of low frequencies. We can see peaks at integer multiples of 50 kHz, but the amplitude of these peaks is an order of magnitude smaller than the noise at low frequencies, so we expect that the lock-in has no significant influence on the reflection signal at the harmonics of the driving frequency.
Also important to note is that in the Fourier transform of the reflection signal of the 50 kHz measurement, shown in figure 22, the harmonic at 600 kHz, the highest harmonic detectable with our sampling rate, is still clearly distinguishable from noise. We therefore expect harmonics at even higher frequencies to be present and cause some aliasing in our recorded data. This effect is even more visible in figure 24, showing the Fourier transform of the reflection signal at a driving frequency of 200 kHz. However, in our measurement at 212.7 kHz (Fourier transform shown in figure 26), the harmonics higher than our acquisition frequency do not overlap with the lower harmonics, and we can manually undo the aliasing if we assume that there are no natural signals at those frequencies. By doing so we can reconstruct the reflection signal, and we present the result below:

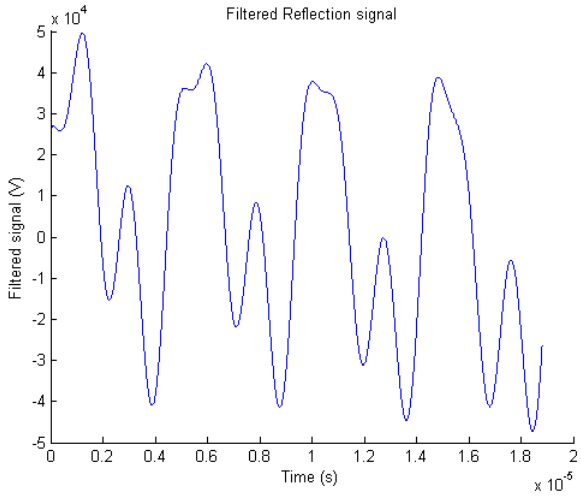

Figure 34: Reconstructed reflection signal while the piezo is oscillating with a sine wave with a frequency of 212.7 kHz and an amplitude of 1.5 nm (3 nmpp).

We will compare this graph with the result from the simulation, i.e. with figure 10 from subsection 6.2. This image is also presented below:

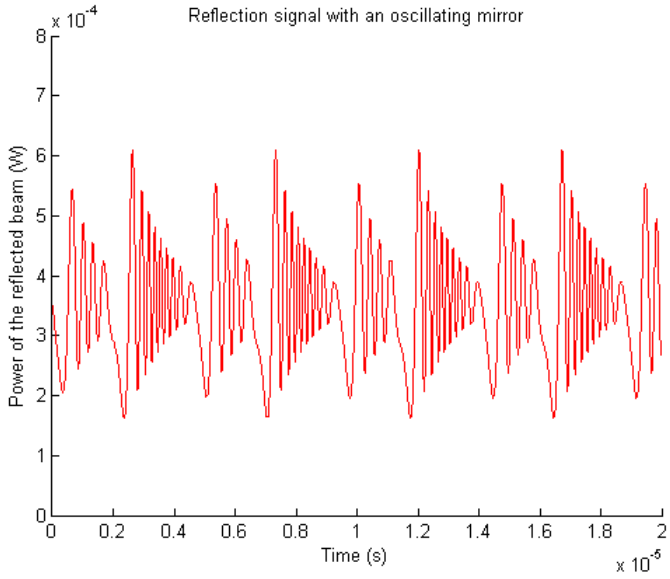

Figure 35: Simulation of the power of the reflected beam (derived from $A(t)$ using the formulas presented in subsection 6.2) when we force the piezo to oscillate at 212.7 kHz. This figure is identical to figure 10.

We note that the two figures are not a perfect match. We will consider their similarities and differences. In the simulation we see many quick oscillations, contained in a larger oscillation. This larger oscillation consists of alternating segments of large amplitude and smaller amplitude. In the data recorded in the experiment the very quick oscillations are not visible, but we do see the large oscillation as well as the alternating amplitude of this large oscillation. In the experiment however, the amplitudes of the two segments of the slow oscillation differ more from eachother than the relative amplitudes found in the simulation.

A possible explanation for the difference in relative sizes as well as a (partial) explanation for the number of peaks is the uncertainty in the value of the detuning Δ in the simulation. We have used a value of Δ of -1 MHz. However, the laser locking to the cavity (fixing Δ) is locked to an intensity set-point on the transmission curve of the cavity, so the actual value of Δ in the experiments is uncertain. Δ effects both the relative size of the peaks and the number of oscillations per large or small oscillation.
Furthermore it should be noted that, using our Fourier filtering, we are attempting to interpolate our measured data on timescales smaller than the acquisition time. There are three possible effects that might cause very high-frequency oscillations to be misrepresented through this analysis. Firstly windowing has significant influence on the results

acquired with this numerical filtering, and in our data we can see (upon closer zoom) that there is some windowing around each peak. Secondly there is some measurement error in the driving frequency of 212.7 kHz. By numerically finding the n'th higher harmonic by multiplying this frequency by n we also multiply this error, and for very high harmonics it is possible that this error becomes so large that the resonance no longer falls within the window of our analysis and is ignored. Thirdly the electronics and detector used contain some low-pass filters, and signal from very high frequencies might have been damped.
Lastly and most importantly the laser we used as the light source in our experiment has a bandwidth of approximately 150 kHz. A possible explanation for the absence of a fast oscillation in the measured data would be this bandwidth. Each component of the light (i.e. each frequency) has a reflection response similar to the one shown in the simulation, but amongst other things the phase and period of the fast oscillation depend on the exact frequency of the source light. It is possible that, when sending in light with a non-zero bandwidth, the fast oscillations destructively interfere to show only the quick oscillations. This would explain the absence of fast changes in our measurement.

10 Comparison to literature

In this section we will compare our results with the results found in literature on this system and similar systems.

In subsections 4.1 and 4.2 we have shown that the differential system contains one or three critical points, and that in the regime with three critical points two of them are stable and one is unstable, so the regime is bistable. In the literature [13, 9] existence of a bistable regime is mentioned, and our results from above and their presented results are in agreement.
However, several articles [9, 10] mention that for positive values of Δ the system presented above leads to heating of the system, rather than cooling. Since convergence to a fixed point implies cooling (as all motion will be slowed down) this is not what we expect from our analysis of the critical points. A possible explanation for this discrepancy would be the existence of stable limit cycles. Solutions with little initial energy (low $|A|$ and $|v|$) would then be attracted to the limit cycle with a higher energy, which corresponds to heating. This idea is supported by [13], which mentions the existence of limit cycles for positive values of Δ.
Lastly we find that many articles [9, 13, 14, 15] mention chaotic behaviour in our system, which might be related to the Hopf bifurcations we have found in subsection 5.3.

11 Conclusion

11.1 Summary of results

In this subsection we summarise the main results from the thesis.

In subsections 4.1 and 5.1 we have found all critical points of the difference and differential system respectively. From this we have concluded that the unstable anti-stokes regime contains stable critical points (section 10). We have found that the solutions of the two different systems describing the experiment are in good agreement (subsection 6.1). In subsections 4.1 and 4.2 we have shown the existence of a bistable regime, and in subsection 6.3 we have numerically shown that this regime will not be reached in experiments as it requires unrealistically large powers ($|B|^2 > 10^6$ W). Lastly we have shown the existence of Hopf bifurcations (subsection 5.3).

Experimentally we have shown the transverse modes that fit inside the cavity (section 8). After this we have measured the response of the system when we force the mirror to oscillate (section 8), and we conclude that the experiment and the theory seem to agree, but improvements to the setup would be able to shed more light on this (section 9).

11.2 Suggestions for future research

In this subsection we will present several possible additions to the work presented in this thesis:

- In subsection 5.3 we have shown that the differential system contains Hopf bifurcations, which have major impact on the dynamics of the system. It would be interesting to know more about these Hopf bifurcations, such as closed formulas for their exact locations (in terms of Δ and $|B|$, or of Δ_c and x_c) as well as numerical or experimental confirmation of chaos.
- For large values of $|B|$ the differential system becomes inaccurate as, among other assumptions, $|x|$ becomes so large that during the experiment the displacement becomes as large as a full spectral range (i.e. we no longer have $\omega \approx \omega_n$ but rather find $\omega \approx \omega_{n+1}$ after a long time). This is explained in more detail in appendix A. The difference system, on the other hand, suffers from problems in that it represents light as bouncing objects rather than a field. A way to improve on both would be to derive the actual system from a classical Hamiltonian.
- We have used a simulation to check the stability of the differential system on large sections of the cubic polynomial presented in subsection 5.2. A suggestion for future

research would be to conduct a more thorough, analytical investigation of these regimes.

- The existence and behaviour of possible limit cycles mentioned in section 10 is of major importance for the long-term behaviour of the system. It would be interesting to extend the search for critical points in this system to limit cycles.

- By increasing the detection speed of the setup it would become possible to detect all overtones (higher harmonics) of the driving frequency, while still keeping this frequency sufficiently high to not disrupt the laser lock. We therefore recommend attempting this again with a faster detection device.

- A more sophisticated method of locking the laser to the cavity is the Pound-Drever-Hall technique [16], which has the advantage of operating at frequencies that differ from the frequency of the signal. Implementing this technique would allow measuring at lower driving frequencies for the piezo. This way it would be possible to measure more harmonics of the signal.

- By repeating the experiment with a cavity with a higher finesse we would be able to measure in a completely different regime, the side-band resolved regime. This is caused by the relative size of Ω_m to the linewidth of the cavity, which at low finesse requires too large a mechanical frequency to measure within a practical acquisition bandwidth. The measurement of macroscopic superpositions will be done in the side-band resolved regime, so investigating this regime will be necessary.

- By using a source with a smaller bandwidth it would be possible to reduce interference between the quick oscillations in our driven experiment, and possibly observe the quick oscillations in the reflection signal.

- In the future it would be interesting to measure the system without manually oscillating the mirror, with the complete opto-mechanical coupling, working two ways, in place.

A Incompatible solutions

In chapter 3 we have derived two different systems describing the behaviour of the Fabry-Pérot cavity with the movable mirror - a system of differential equations and a system with a difference equation. In this chapter we will show that these two different systems will under some circumstances indeed give rise to different behaviour by considering the number of critical points of each system. Also we will explain which approximation in the derivation of the differential equation causes this difference in critical points.

We have shown at the end of subsection 5.2 that, depending on the values of Δ and $|B|^2$, the differential system has 1 or 3 critical points. At the end of subsection 4.2 we argue that the number of critical points of the system with the difference equation can be far larger, which we will show in more detail here. We find at the end of subsection 4.2 that any positive solution x_c of the equation given below gives us a critical point of the differential system:

$$x_c \left(\cosh\left(2\alpha(L+x_c) - \log(r_1 r_2)\right) - \cos\left(2\frac{\omega}{c}(L+x_c)\right)\right) = \frac{|B|^2|t_1|^2}{2r_1 r_2 Y}.$$

Setting $\alpha = 0$, $r_1 = r_2 = \sqrt{1-\epsilon}$ and $r_1^2 + t_1^2 = r_2^2 + t_2^2 = 1$ we find that the above can be written as:

$$x_c \left(\frac{1}{2}\left(1 - \epsilon + \frac{1}{1-\epsilon}\right) - \cos\left(2\frac{\omega}{c}(L+x_c)\right)\right) = \frac{|B|^2\epsilon}{2(1-\epsilon)Y}.$$

If we now assume that ϵ is small (which is the case for good mirrors) we can rewrite the above as:

$$x_c \left(\left(1 + \frac{1}{2}\epsilon^2 + O(\epsilon^3)\right) - \cos\left(2\frac{\omega}{c}(L+x_c)\right)\right) = \frac{|B|^2\epsilon}{2Y} + O(\epsilon^2).$$

If we look at the left-hand-side, we see that the term between the outer brackets is oscillating between 2 and $\frac{1}{2}\epsilon^2$, and therefore the whole left-hand-term is oscillating between $2x_c$ and $\frac{1}{2}\epsilon^2 x_c$. We therefore expect to be able to find solutions as long as $2x_c > \frac{|B|^2\epsilon}{2Y} > \frac{1}{2}\epsilon^2 x_c$, which is equivalent to $\frac{|B|^2\epsilon}{4Y} < x_c < \frac{|B|^2}{Y\epsilon}$. If we pick ω large then the term between the brackes on the left-hand-side will oscillate between its maximum and minimum many times in this interval, and the whole l.h.s. will interset the constant r.h.s. at least once every oscillation. Therefore there will be a large number of critical points under these circumstances.

Under the circumstances mentioned above (α small, ω large, $r_1, r_2 \approx 1$) we see that the differential system has at most 3 critical points, whereas the system with the difference equation has a large number of critical points, and the value of x_c greatly values over these critical points. In particular there are critical points of the difference system which are far from any critical point of the differential system. Around such a point the local dynamics of

the difference system will be determined by the nature of the critical point (i.e. exponential approach to/retreat from the critical point), whereas this cannot be the case for the differential system (as this would imply the existence of a critical point in the neighbourhood).

The reason these two systems give different dynamics under these circumstances is due to the expansion $\omega = \omega_n + \Delta$ with $|\Delta| \ll \omega_n$ in the derivation of the differential system, combined with the assumption that $|x|$ is small. In the difference system we can find a multitude of critical points with the values of x_c placed approximately $\frac{2\pi}{2\frac{\omega}{c}} = \frac{\pi c}{\omega}$ distanced apart. However, increasing x by a distance $\frac{\pi c}{\omega} \approx \frac{\pi c}{\omega_n}$ is equivalent to increasing L by this same distance and increasing n by one, as we will show below. Let $\omega_n(L) = \frac{\pi n c}{L}$, our claim is that $\omega_n(L) = \omega_{n+1}\left(L + \frac{\pi c}{\omega_n(L)}\right)$. We see that:

$$\begin{aligned}
\omega_{n+1}\left(L + \frac{\pi c}{\omega_n(L)}\right) &= \frac{\pi(n+1)c}{L + \frac{\pi c}{\frac{\pi n c}{L}}} \\
&= \frac{\pi(n+1)c}{L + \frac{L}{n}} \\
&= \frac{n+1}{1+\frac{1}{n}}\frac{\pi c}{L} \\
&= \frac{\pi n c}{L} = \omega_n(L)
\end{aligned}$$

We conclude that increasing x_c by the amount needed to locate the next critical point of the difference system is equivalent to picking a different value of L as the average position and increasing n by one. Since we fix n in the derivation of the differential equation this latter action is not possible in our later system, and therefore we only find the critical points around one fixed L and n. This explains the difference in critical points for the two systems, and also shows that indeed the differential system is a valid approximation only when $|x| \ll \frac{1}{2}\lambda_n = \frac{L}{n}$. If this condition is met we expect the two systems to be in good agreement, as is also shown in subsection 6.1.

B Mode-matching

An experimental aspect not covered in the theory presented earlier is the quantization of states of propagating light from a laser. Light is best described by Maxwell's equations. Searching for solutions of Maxwell's equations in free space that resemble straight beams and can be emitted from a laser yields a collection of modes, the most important of which is the fundamental TEM_{00}-mode. Light in this mode has the same form as a Gaussian beam, which means that light moves in a straight line and on a cross-section perpendicular to the axis of propagation the intensity profile is a 2D Gaussian. If we call the axis of propagation the z-axis a Gaussian beam is fully determined by a complex function $q(z)$, which describes the beam radius and shape of the phase front along the axis of propagation.

Solving Maxwell's equations for the inside of a Fabry-Pérot cavity yields again a collection of modes. Along the propagation axis there are the multiple resonance frequencies, but perpendicular to the propagation axis the modes are also discrete. The cavity modes resemble the free space modes found earlier, and for simplicity's sake we will try to transform our light outside the cavity (in a TEM_{00}-mode) into the Gaussian (fundamental) cavity mode. This Gaussian mode inside the cavity has a known function $q(z)$, which can be calculated using the cavity optics formulas in [1, p. 750]. Our goal is to make the $q(z)$ of the beam outside the cavity coincide with the $q(z)$ of the Gaussian cavity mode through the use of lenses.

We first need to know $q(z)$ from the optical fibre coming from the laser. To do this we place a lens ($f = 400$ mm) after the fibre end, and we find a beam waist roughly 40 cm along the axis of propagation. We know from [17] that:

$$\frac{1}{q(z)} = \frac{1}{R(z)} - i\frac{\lambda}{\pi w(z)^2}.$$

Here $R(z)$ is the radius of curvature of the wavefront, and $w(z)$ is the radius of the Gaussian profile (i.e. at a distance of $w(z)$ from the center of the beam the amplitude of the wave is $\frac{1}{e}$ of its amplitude at the center. This is $\sqrt{2}$ times the standard deviation of a Gaussian curve). At the waist of a beam the wavefront is flat, so $R(z) = \pm\infty$ and q is fully determined by the beam radius $w(z)$, which we have measured to be 0.25 cm ± 0.1 cm. Next we calculate our $q(z)$ for the cavity mode, using the formulas from [1]. Since our cavity is symmetrical about its center the fundamental mode has a beam waist in the center of the cavity. The radius at this center is determined by:

$$w_0^2 = \frac{L\lambda}{\pi}\sqrt{\frac{1+g}{4(1-g)}} = 5.08 \cdot 10^{-8}\ \text{m}^2.$$

Here $g = 1 - \frac{L}{R}$ with R the radius of curvature of the mirrors at the ends of the cavity and L is the distance between the two mirrors.
Our goal is to place lenses in between our measured beam waist and the center of the cavity

in such a way that the $q(z)$ from the laser coincides with the q of the cavity mode. In order to do this we need to make sure that the real and the imaginary parts coincide, so we need two degrees of freedom to ensure this. In our setup we chose to place an extra lens in the beam path, and the two degrees of freedom will be the position and focal length of the lens. In practice it might be easier to add two lenses to the setup and use their positions as tuneable parameters. A schematic overview of the system of lenses is presented below:

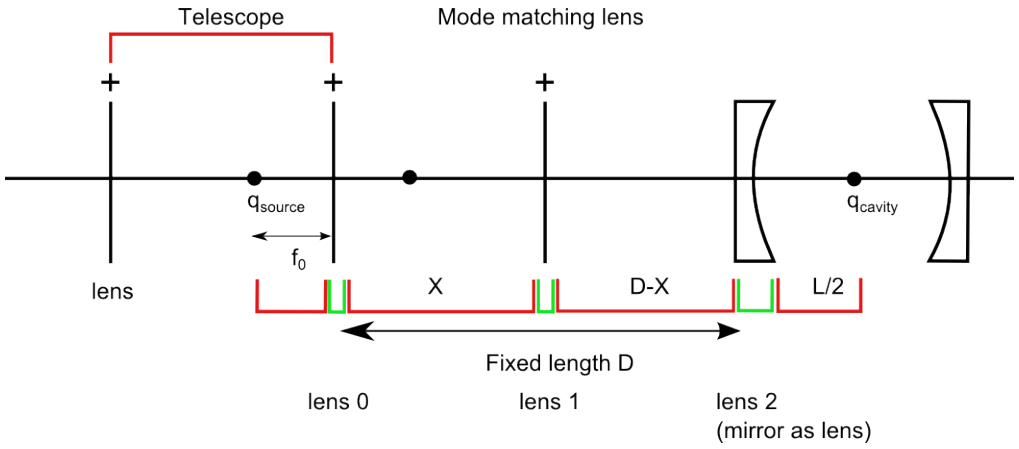

Figure 36: A schematic overview of the collection of lenses used to match the mode of the source to the cavity mode.

Using the ray optics matrices described in [17] we can write our problem as the following equation:

$$(cm)\begin{pmatrix} q_{\text{cavity}} \\ 1 \end{pmatrix} = \begin{pmatrix} 1 & \frac{L}{2} \\ 0 & 1 \end{pmatrix}\begin{pmatrix} 1 & 0 \\ -\frac{1}{f_2} & 1 \end{pmatrix}\begin{pmatrix} 1 & D-X \\ 0 & 1 \end{pmatrix}\begin{pmatrix} 1 & 0 \\ -\frac{1}{f_1} & 1 \end{pmatrix}\begin{pmatrix} 1 & X \\ 0 & 1 \end{pmatrix}\begin{pmatrix} 1 & 0 \\ -\frac{1}{f_0} & 1 \end{pmatrix}\begin{pmatrix} 1 & f_0 \\ 0 & 1 \end{pmatrix}\begin{pmatrix} q_{\text{source}} \\ 1 \end{pmatrix}$$

Here, as shown in the picture, f_0 is the focal length of the first lens, f_1 is the focal length of the second lens and f_2 is the focal length of the first mirror (which acts as a negative lens on the light that is transmitted through it). D is the distance between the cavity and the first lens, X is the distance between the second lens and the first lens and L is again the length of the cavity. The (cm) stands for 'cancel me' and is a constant (in ray optics only the ratio of the two elements in the vector is acted upon, and by introducing the (cm)-term we can rewrite the ray optics as a system of linear equations). We wish to solve this by tuning X and f_1, keeping all other variables fixed. This could be done by expanding the linear equations above, dividing the top equation by the bottom one to eliminate the (cm)-term, splitting the resulting equation into real and imaginary part, solving the system of equations for $\frac{1}{f_1}$ (as the resulting equations are both linear in this variable) and determining X from the resulting equation. In practice we used a computer simulation, varying X and determining f_1 from the equations above, and searching for an

X for which f_1 is real. We ran this simulation for different values of q_{source} to accommodate measurement errors, giving us the following table of results:

Table 2: Table of position and focal length of mode-matching lens. For this set of simulations we used $f_0 = 10$ cm, $D = 1$ m, $f_2 = -100$ cm, $L = 10$ cm, $w_{\text{cavity}} = 2.19 \cdot 10^{-4}$ m and $\lambda = 10^{-6}$ m. All of these values have been determined from the actual setup.

w_{source} (cm)	X (cm)	f_1 (cm)
0.15	59.0	26.1
0.20	52.4	24.9
0.25	47.3	23.6
0.30	43.2	22.3
0.35	39.9	21.0

From this we concluded that we needed a lens with a focal length of 25 centimeters, and the position would have to be determined in the actual setup. To get a better estimate of the correct placement of the lens and of the sensitivity to misalignment we ran a second simulation where f_1 was fixed at a value of 25 cm, and we determined the $q(z)$ at the center of the cavity as a function of X. The results are shown in the graphs below:

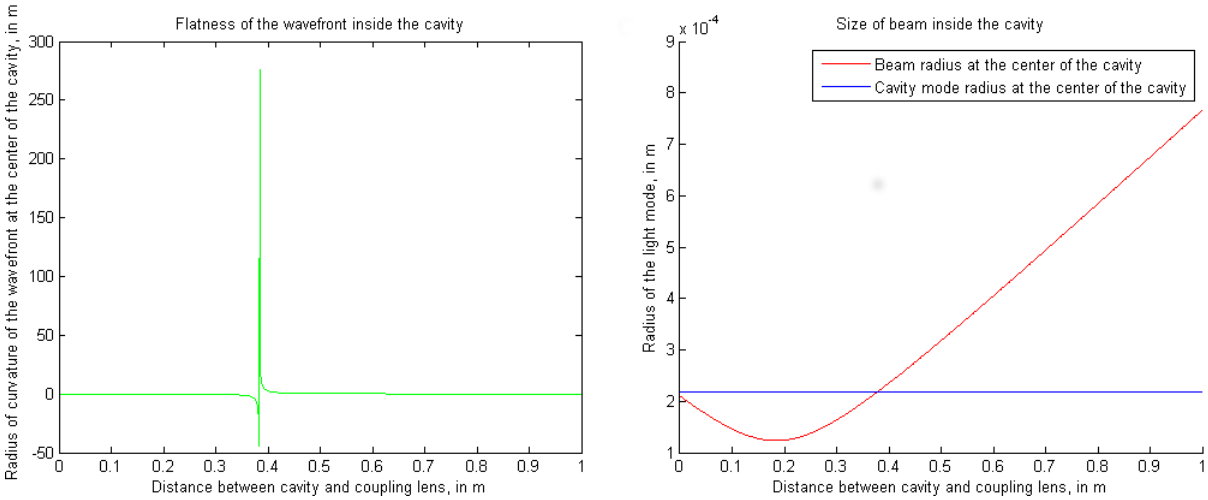

Figure 37: The radius of curvature of the wavefront and the radius of the beam at the center of the cavity, as a function of $D - X$. Here $f_0 = 10$ cm, $f_1 = 25$ cm, $f_2 = -100$ cm, $D = 1$ m, $L = 10$ cm, $w_{\text{cavity}} = 2.19 \cdot 10^{-4}$ m (as shown in the graph) and $\lambda = 10^{-6}$ m. The actual cavity mode has a beam radius of w_{cavity} and a radius of curvature of $\pm\infty$.

From these graphs we conclude that by placing the coupling lens at $X \approx 62$ cm the coupling into the fundamental cavity mode should be decent.

References

[1] A. E. Siegman, *Lasers* (University Science Books, Sausalito, California, 1986).

[2] G. Brooker, *Modern Classical Optics* (Oxford University Press, Oxford, 2003).

[3] A. L. Schawlow and C. H. Townes, Physical Review **112**, 1940 (1958).

[4] K. Taylor and P. D. Atherton, Monthly Notices of the Royal Astronomical Society **191**, 675 (1980).

[5] P. Jacquinot, Journal of the Optical Society of America **44**, 761 (1954).

[6] B. Abbott *et al.*, Nuclear Instruments and Methods in Physics Research Section A: Accelerators, Spectrometers, Detectors and Associated Equipment **517**, 154 (2004).

[7] D. Kleckner and D. Bouwmeester, Nature **444**, 75 (2006).

[8] J. D. Teufel *et al.*, Nature **475**, 359 (2011).

[9] M. Aspelmeyer, T. J. Kippenberg, and F. Marquardt, arXiv e-print 1303.0733 (unpublished).

[10] T. J. Kippenberg and K. J. Vahala, Optics Express **15**, 17172 (2007).

[11] W. Marshall, C. Simon, R. Penrose, and D. Bouwmeester, Physical Review Letters **91**, 130401 (2003).

[12] S. E. Strigin and S. P. Vyatchanin, Gravitation and Cosmology **17**, 87 (2011).

[13] F. Marino and F. Marin, Physical Review E **87**, 052906 (2013).

[14] T. Carmon, H. Rokhsari, L. Yang, T. J. Kippenberg, and K. J. Vahala, Physical Review Letters **94**, 223902 (2005).

[15] T. Carmon, M. C. Cross, and K. J. Vahala, Physical Review Letters **98**, 167203 (2007).

[16] E. D. Black, American Journal of Physics **69**, 79 (2001).

[17] H. Kogelnik and T. Li, Proceedings of the IEEE **54**, 1312 (1966).